energies

MDPI

Article

New Topology of a Hybrid, Three-Phase, Four-Wire Shunt Active Power Filter

Stefani Freitas [1,*], Luis Carlos Oliveira [2], Priscila Oliveira [1], Bruno Exposto [3], José Gabriel Pinto [3] and Joao L. Afonso [3]

[1] Campus de Palmas, Federal University of Tocantins, Palmas 77001-090, TO, Brazil
[2] Faculty of Electrical Engineering, State University of São Paulo, Ilha Solteira 05508-060, SP, Brazil
[3] ALGORITMI Research Centre/LASI, University of Minho, 4800-058 Guimarães, Portugal
* Correspondence: stefaniclf@uft.edu.br

Abstract: With a view to reducing harmonic content in electrical power systems, and, consequently, improving power quality level, filters and other harmonic compensation devices are widely used. In the category of filters, they can be distinguished into two classes that are related to the operating mode, active or passive, both widely known and applied in electrical power grids and in the most diverse industry sectors. In this sense, taking into account the use of compensating devices in four-wire electrical systems feeding single-phase, non-linear loads, this paper presents a new hybrid arrangement of harmonic compensation that incorporates both active and passive filtering, which performs all functions concerning the harmonic compensation of a four-leg shunt active power filter. In this hybrid arrangement, the harmonic filtering of positive and negative sequence components is performed by a three-leg shunt active power filter, while the filtering of zero-sequence harmonics is attributed to the electromagnetic zero-sequence suppressor. The results, which confirm the effectiveness of the proposed hybrid arrangement, are proven through simulations and experimental tests in different operating scenarios, revealing a substantial improvement in the system's power factor, as well as a reduction in harmonic distortions.

Keywords: electromagnetic suppressor; harmonics; power factor; shunt active power filter

check for updates

Citation: Freitas, S.; Oliveira, L.C.; Oliveira, P.; Exposto, B.; Pinto, J.G.; Afonso, J.L. New Topology of a Hybrid, Three-Phase, Four-Wire Shunt Active Power Filter. *Energies* **2023**, *16*, 1384. https://doi.org/10.3390/en16031384

Academic Editor: Alon Kuperman

Received: 27 December 2022
Revised: 20 January 2023
Accepted: 23 January 2023
Published: 30 January 2023

Copyright: © 2023 by the authors. Licensee MDPI, Basel, Switzerland. This article is an open access article distributed under the terms and conditions of the Creative Commons Attribution (CC BY) license (https://creativecommons.org/licenses/by/4.0/).

1. Introduction

In the search for competitiveness in the global markets, many industrial and power-generation segments are using state-of-the-art equipment and control systems in their production lines [1–4]. In this context, most of the electrical loads are non-linear devices. These devices are associated with the more efficient use of electrical energy and control process optimization [5–8]. From these perspectives, the harmonic currents generated by predominantly industrial consumers are increasingly being added to those emitted by residential consumers and those in the service sector, systematically contributing to the loss of power quality of the electrical energy available [9–15].

Aiming to mitigate harmonic distortion, and, consequently, improve the power factor in systems, whenever possible, operational measures normally related to the suitability of loads are adopted, making use of fewer grid-polluting technologies, multiplying the number of switching pulses in large converters, and changing the topology of electrical networks, among other things. It happens, however, that, on several occasions, such measures are unfeasible from an economic point of view or even insufficient to guarantee the proper operation of the system and/or meet the limits established by the standards and technical recommendations [16,17]. In these cases, it is essential to use special equipment to mitigate the harmonic distortion of power grids and electrical installations.

Solutions involving passive, active, or hybrid power filters are employed with the aim of reducing or even eliminating the problems caused by harmonic currents, as presented in [18–33].

The most common shunt active power filters (ShAPF) are equipment based on the use of a voltage source inverter with current control with a capacitor on the DC side to act as a current source, and the topologies used can have three or four arms composed of six or eight electronic switches, respectively.

The three-phase systems that supply balanced loads and that do not present harmonic current multiples of three do not require compensation of zero-sequence power. In these conditions, a simple inverter with only three arms [34–36] is sufficient to provide the compensation currents and guarantee the correction of harmonic distortions of the supply currents, unbalances, and power factor. This solution requires only four current sensors and has a simpler control system.

The topology of a four-arm shunt active filter (ShAPF-4) is applied in three-phase systems with a neutral wire and can be used to compensate harmonics and correct the power factor, in addition to balancing the load currents, even with single-phase loads. However, this solution requires the use of eight power switches and needs six current sensors and four voltage sensors to supply the necessary data for the control system, which is also more complex than in the previous case.

Considering, therefore, the expectation of application of compensating structures in four-wire electrical systems with single-phase loads, it is intended to use in this work a ShAPF with a lower cost, i.e., a topology with three arms (ShAPF-3) containing only six power switches. This topological simplification leads to the use of a smaller number of current and voltage sensors, as well as simplifying the control. However, when faced with single-phase, linear or non-linear loads, the compensation of the zero-sequence components cannot be performed. Under these conditions, it is intended to perform the compensation of the homopolar components by means of a zero-sequence electromagnetic suppressor (ZSS) [20] composed of a zero-sequence filter (ZSF) [27] and a zero-sequence blocker (ZSB) [28], which are simple, robust, and reliable passive structures, with mastered technological knowledge and well-defined costs.

Particularly, as a specific objective of this work, it is intended, therefore, to continue the preliminary studies carried out in previous works [20,34], investigating through theoretical considerations, simulations, and experimental tests the performance of this new hybrid structure of harmonic filtering.

This paper presents a complete study of this hybrid filter and is organized as follows: Section 2 presents the theoretical and mathematical considerations of the ZSS and ShAPF; Section 3 presents simulation results of the hybrid arrangement; in Section 4, the experimental results of the hybrid filter operation in different operating conditions are presented; finally, Section 5 presents the main conclusions of this study.

2. Hybrid Filter

The following sections present the functionalities of the ZSS and the ShAPF that constitute the hybrid, three-phase, four-wire shunt active power filter (HyShAPF), as well as the operation of these devices in the mitigation of harmonic currents generated by non-linear loads.

2.1. Electromagnetic Zero-Sequence Supressor (ZSS)

The so-called ZSS, investigated in detail in [20], is formed by the composition of a ZSF connected in parallel to the distribution system and a ZSB connected in series, as shown in Figure 1. The electromagnetic arrangement of the ZSB is formed by three windings juxtaposed in the central column of the magnetic core. The filter arrangement is composed of two recognized coils called main and auxiliary, arranged on the same column of the magnetic core, connected in a zigzag pattern. This denomination of the coils, main and auxiliary, does not imply their importance level, since it is used only to identify each set of coils.

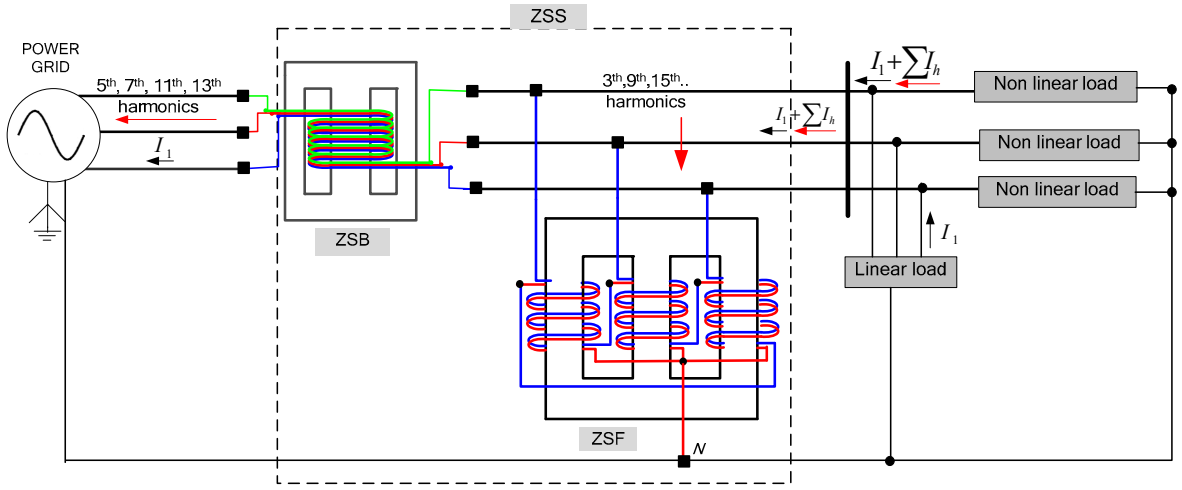

Figure 1. Zero-sequence suppressor (ZSS) composed by the zero-sequence filter (ZSF) and the zero-sequence blocker (ZSB).

The purpose of the ZSF connected in parallel to a harmonic-generating load is to offer a means for the homopolar harmonic components to be restricted to the circuit composed of the load and the filter, with no change in the harmonic content produced by the load but rather a detour in the circulation path. Thus, the operating efficiency of the ZSF depends on the proportion between its zero-sequence impedance and the respective system impedance at the point of common coupling (PCC) [27]. In this sense, the ZSB, which is a zero-sequence, high-impedance device, works as an impedance adapter, cooperating to maximize the operation of the ZSF and blocking the passage of zero-sequence harmonic currents from the load to the source. Therefore, the effectiveness of the ZSF is greater the smaller its zero-sequence impedance against the respective system impedance at the PCC. In this context, the main function of the ZSB is to adapt the total impedance in the PCC seen by the filter, aiming for a performance of the ZSF in line with the mandatory standards [20–27].

In terms of the physical constitution of the ZSF and the ZSB, it is essentially a coupling with the minimum number of dispersions, which maximizes their functionalities.

In this sense, for the ZSB to block the zero-sequence by providing a high equivalent inductance, and, simultaneously, a low equivalent inductance for positive and negative sequences, it is necessary to obtain a maximum unitary coupling between the coil windings ($\lambda_b = 1$) in such a way that the self-inductances, L_b, and mutual inductances, M_b, are very similar. Equation (1) relates the self- and mutual inductances through a coupling factor, λ_b. Then:

$$M_b = \lambda_b \, L_b \tag{1}$$

where:

λ_b—coupling factor between electromagnetic blocker coils;

L_b—self-inductance of blocker coils.

Thus, for the zero-sequence, the self- and mutual inductances are summed, causing an inductance that is three times greater. The opposite happens for the positive and negative sequences, and the self- and mutual inductances cancel each other out, forming a free path for these components. Assuming, therefore, equality between the inductances of each coil, L_b, and between the mutual inductances of different phases coils, M_b, the following expressions of the sequential voltages are obtained (Equations (2) and (3)).

$$V_{1,2}^h = j\omega h[L_b - M_b]I_{1,2}^h \tag{2}$$

$$V_0^h = j\omega h[L_b + 2M_b]I_0^h \tag{3}$$

Figure 2 illustrates the equivalent sequential circuit analysis for an ideal coupling between the coils.

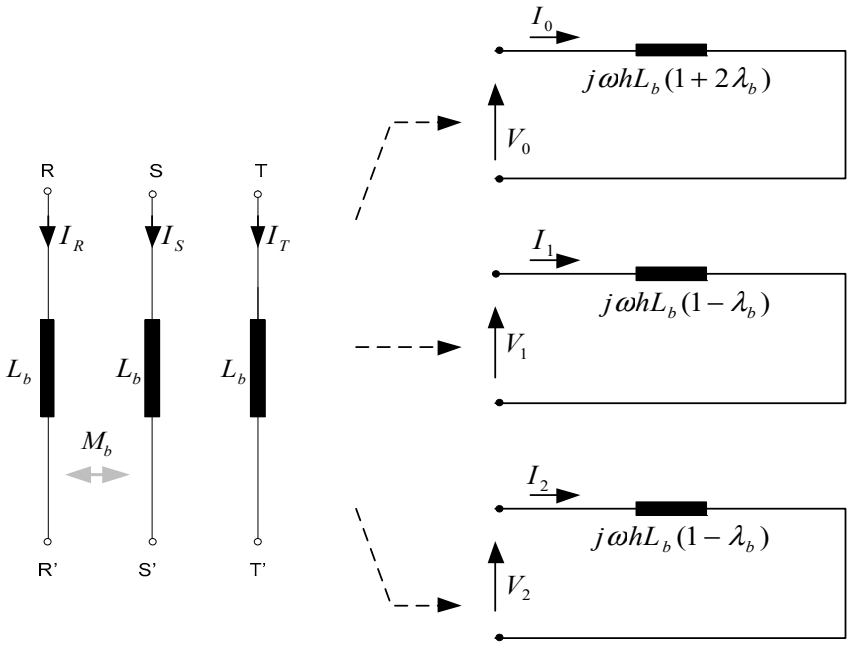

Figure 2. Blocker decoupled sequential circuits.

These characteristics reveal the blocking action to zero-sequence components, the effectiveness of which is proportional to the coupling factor, which is ideally of unitary value.

In the ZSF, as the mutual inductance value between the main and auxiliary coils of the same column, M_f, approaches the value of the coils' self-inductance, L_f, the zero-sequence equivalent inductance tends to be the minimum value. Ideally, these inductances are related, as shown in Equation (4).

$$M_f = \lambda_f \sqrt{L_{Pf} \quad L_{Af}} \tag{4}$$

where:

λ_f —coupling factor between the coils of the same column of the ZSF;
L_{Pf} —self-inductance of the main winding;
L_{Af}—self-inductance of auxiliary winding.

Therefore, considering the self-inductances of the identical coils, L_f, and the mutual inductances between coils of the same identical column, M_f, we then obtain the equations of the positive and negative sequential voltages (Equation (5)), which are similar since it is a static piece of equipment for zero-sequence voltage (Equation (6)).

$$V_{1,2}^h = j\omega h\left[2L_f + M_f + 3M\right] I_{1,2}^h \tag{5}$$

$$V_0^h = j\omega h\left[L_f - M_f\right] I_0^h \tag{6}$$

Considering the coupling factor between the coils of the same column of the three-phase filter core, the system can be represented through the decoupled sequential circuits illustrated in Figure 3.

For a perfect coupling (λ_f = 1), the inductance for the zero-sequence is null, that is, $M_f = L_f$. It can be said, then, that the proposed device represents a short circuit for all zero-sequence currents and is, therefore, an ideal filter for this sequence.

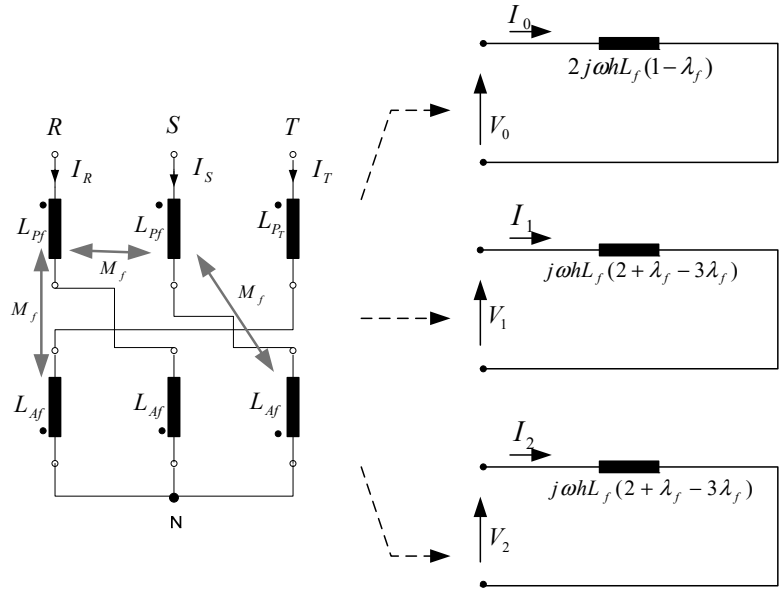

Figure 3. Decoupled sequential circuits.

2.2. Shunt Active Power Filter

The connection of the ShAPF in the electrical power grid is determined by the possible configurations of the power systems. Based on the standards adopted since the beginning of the 20th century, the most common distribution system is the three-phase system, and the inverters can be powered either by a current source or by energy storage elements.

A possible topology for three-phase, four-wire systems is known as a four-leg inverter. For this configuration, the fourth leg is used exclusively for neutral current circulation through the ShAPF. The advantages compared to the topology of another parallel ShAPF, such as the split capacitor, are the lower current effort on the DC bus capacitor and the control system that enables a dynamic performance of the voltage and current control of the filter. The main one is the use of a greater number of semiconductor switches, a fact that increases material costs and makes the control system more complex. Figure 4 illustrates the topology with the four-leg inverter. The equations and development of the ShAPF used for tests in this work can be seen in [34].

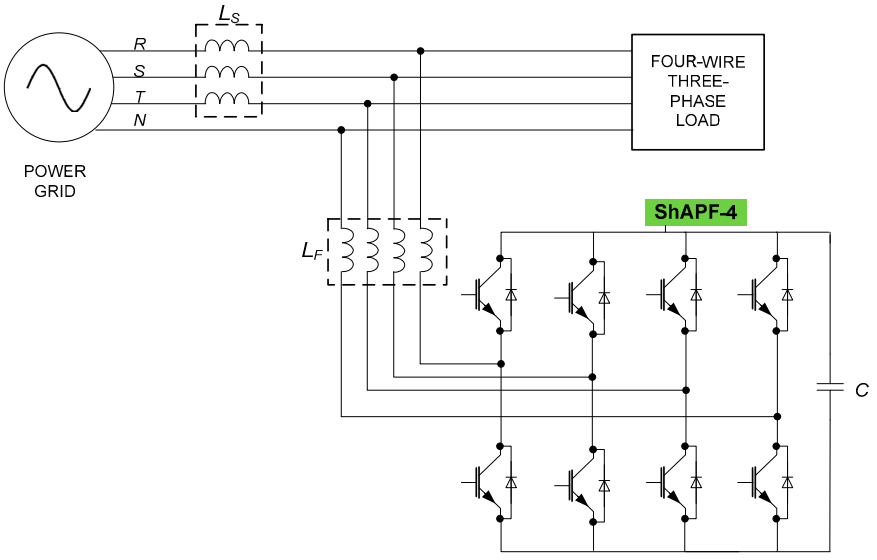

Figure 4. Four-leg ShAPF connected to a three-phase, four-wire system.

The *p-q* theory, proposed by Akagi et al. [37,38], allows the implementation of the ShAPF control system in a simple and effective mode, since the calculations only consist of algebraic operations that can be performed with integer arithmetic [34].

Figure 5 presents the electrical schematic of the ShAPF of this work. It basically consists of an inverter and the control system (controller). From the measurement of the instantaneous values of the phase voltages (V_R, V_S, and V_T) and the load currents (I_{HR}, I_{HS}, and I_{HT}), the controller calculates the reference compensation currents (I_{CR}, I_{CS}, and I_{CT}) for the inverter. Finally, the inverter produces the power factor compensation and harmonic compensation currents (I_{HR}*, I_{HS}*, and I_{HT}*) as the same mode and in phase opposition as the load harmonic currents.

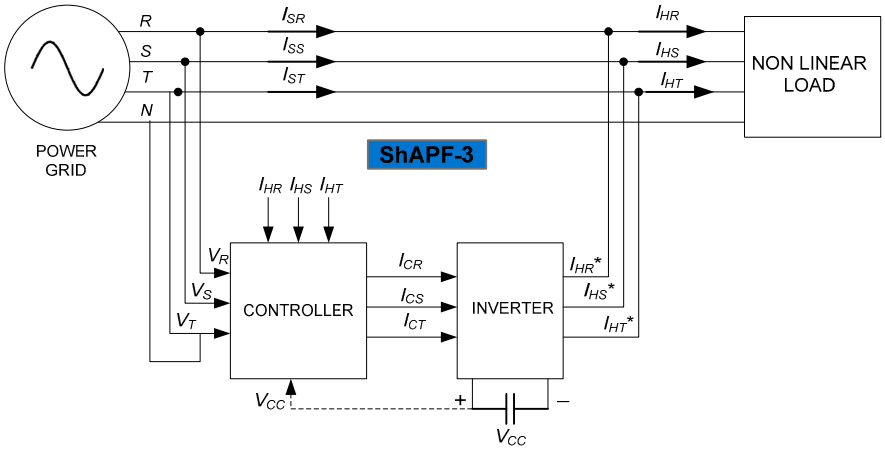

Figure 5. ShAPF block diagram.

2.3. Hybrid Arrangement

Considering the expectation of compensating structure application in four-wire electrical systems with single-phase loads, the possibility of a new arrangement of harmonic compensation which simultaneously incorporates active and passive filtering and which presents all the functionalities in terms of harmonic compensation of a four-leg ShAPF was aspired. From this perspective, a three-leg ShAPF, responsible for filtering the positive and negative sequence components, and a ZSS, which is assigned the function of draining zero-sequence components, are jointly used. In light of the *p-q* theory power components [39,40], the new power flow, provided by the HyShAPF in question in this work, is performed as illustrated in Figure 6. The components $\overline{p_0}$ and $\widetilde{p_0}$, related to the instantaneous zero-sequence power, are drained by the action of the electromagnetic suppressor. The components of power related to the oscillating part of the instantaneous real power, $\widetilde{p}$, as well as the total components of the instantaneous reactive power, q, are compensated by the three-leg ShAPF, even with a single-phase load. It is observed that, ideally, under the joint action of the two devices, only the mean value of the instantaneous real power, $\overline{p}$, and the mean value of the instantaneous zero-sequence power, $\overline{p_0}$, come from the power supply. For this configuration, the harmonic compensation of the ShAPF occurs as in a three-phase, three-wire system, since the responsibility of the fourth wire is transferred to the ZSS.

As previously highlighted, electromagnetic devices are simple and robust structures, for which the knowledge of projects and applications is already mastered with well-defined costs. Considering the same power level to be processed, it is assumed that the costs of electromagnetic devices are lower than those of electronic switches. This relationship can be even more favorable when taking into account the costs related to signal processing and electronic switch control.

Thus, from a topological and operational point of view, all the functionalities of a four-leg ShAPF are achieved using the HyShAPF, composed of a three-leg ShAPF and a ZSS, as shown in Figure 7. Therefore, the proposed new harmonic filtering hybrid arrangement is connected to an electrical system as suggested in Figure 8.

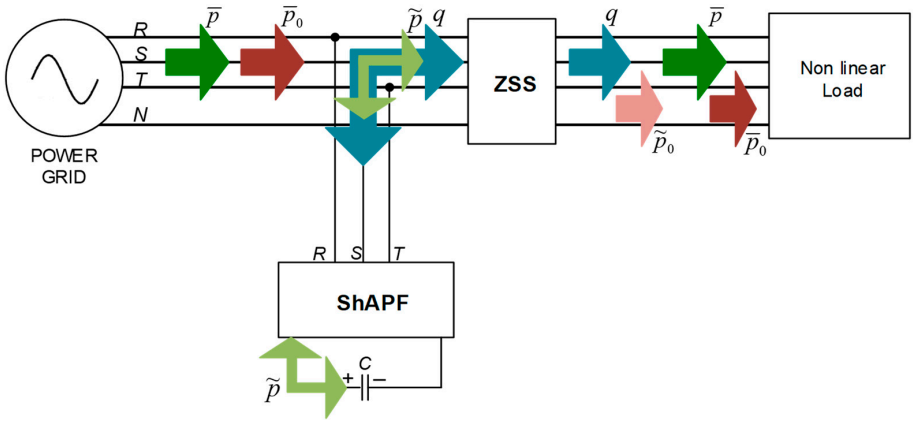

Figure 6. *p*-*q* theory power components using the HyShAPF.

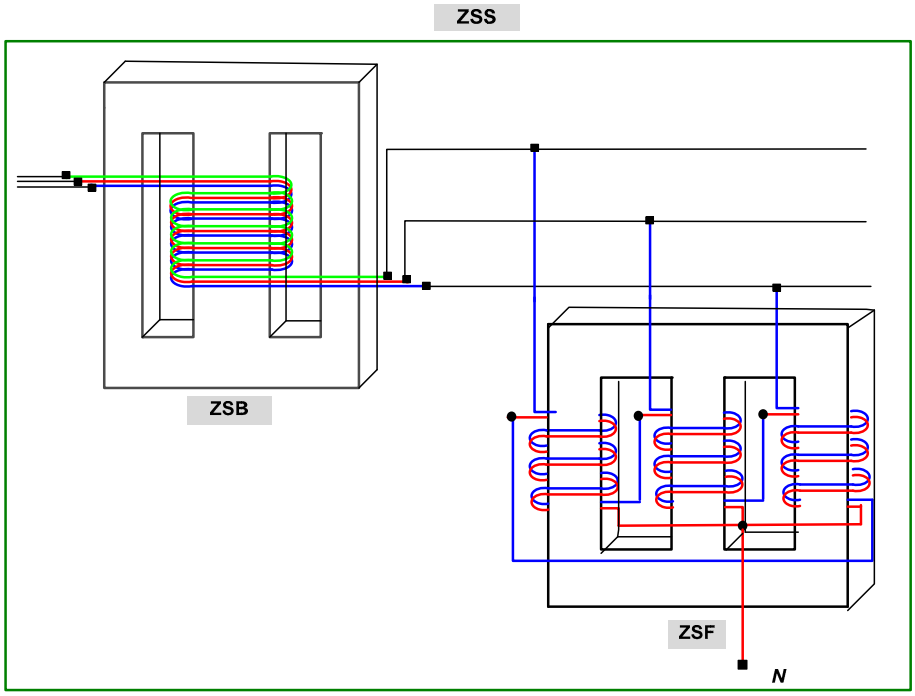

Figure 7. Electromagnetic structure of the zero-sequence electromagnetic suppressor (ZSS).

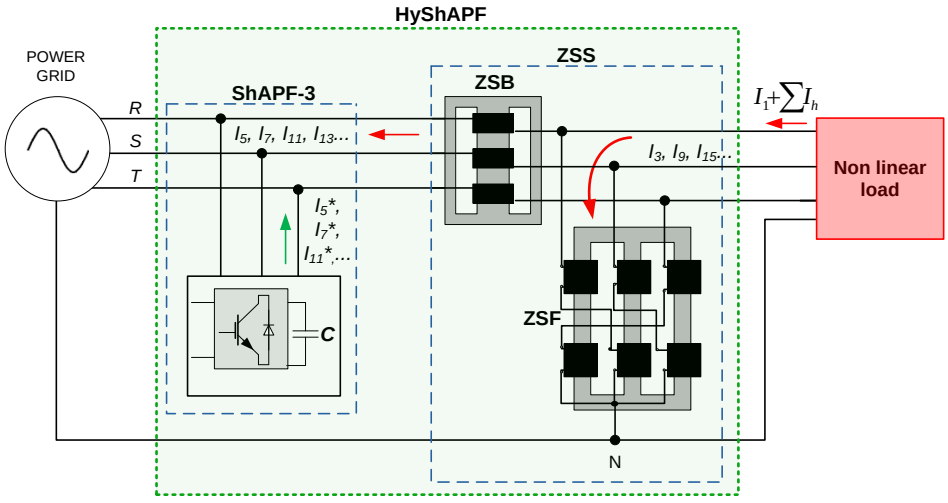

Figure 8. Proposed hybrid filtering arrangement (HyShAPF).

3. Simulation Results

In order to validate the performance of the electromagnetic devices, the ShAPF and the HyShAPF, digital simulation studies were initially performed in PSIM® software. The electromagnetic devices ZSF and ZSB were modeled based on the methodologies proposed in [32] and described in detail in [20]. Basic elements containing mutually coupled inductors from the PSIM® library were used. The construction of the ShAPF also used basic elements from the digital simulation software library, such as diodes, DC source, and inductors. The ShAPF control technique in question was based on the *p-q* theory and can be seen in detail in [34,35].

The procedures for the non-linear load composition followed the same methodology. From the basic elements of PSIM®, two types of loads were configured, three-phase and single-phase. The three-phase load consisted of a six-pulse diode rectifier feeding an RL load. To compose the total load, three diode bridge rectifiers with a capacitive filter feeding a resistive load were chosen. The three-phase load was, therefore, composed of three single-phase loads. To observe the behavior of the compensation system against load imbalance, a timed switch was introduced in the model.

Table 1 presents the data used in the configuration of the elements of the simulated system.

Table 1. Simulated system data.

Parameter	Value
Power grid voltages	≈230 V
Frequency	50 Hz
Electromagnetic filter (ZSF)	L_f = 300 mH; R_f = 0.2 Ω; λ_f = 0.998
Electromagnetic blocker (ZSB)	L_b = 5 mH; R_b = 0.03 Ω; λ_b = 0.998
Single-phase rectifiers with capacitive filter	R = 42 Ω; C = 500 uF
Three-phase rectifier with inductive filter	R = 42 Ω; L = 5 mH
ShAPF DC voltage	750 V

Results in Steady State

The presented simulations were performed for different steady-state intervals, which included topological variations of the filtering system and the non-linear load. The central objective of this analysis was to investigate the sequential distribution of the harmonic components, as well as the unbalance indices before and after the operation of the filtering devices and their combinations. The calculations of the sequential components and the respective discrete Fourier transformer (DFT) were performed using spreadsheets developed in Excel®. For this, 200 samples per cycle for each period of interest were extracted from the simulation results obtained in PSIM®.

A. Balanced, non-linear loads without filters

Figure 9a illustrates the steady-state waveforms of the three-phase currents on source side. On the graph scale, the neutral current was divided five times. This case was taken as a reference for the subsequent analyses of cases B and C. The set of loads, composed of a three-phase rectifier with inductive filter and identical single-phase loads consisting of bridge rectifiers with capacitive filter, presented characteristic harmonic components according to phase and sequential spectrum, as illustrated in Figure 9b,c.

Figure 10 shows, for the same phase, the voltage and the respective current on the source side. To facilitate the visualization of the results, in the graphic scale, the phase current was multiplied five times. The power factor obtained in this case was 0.92 and was fundamentally due to the harmonic distortion of the current, since the fundamental component was practically in phase with the voltage.

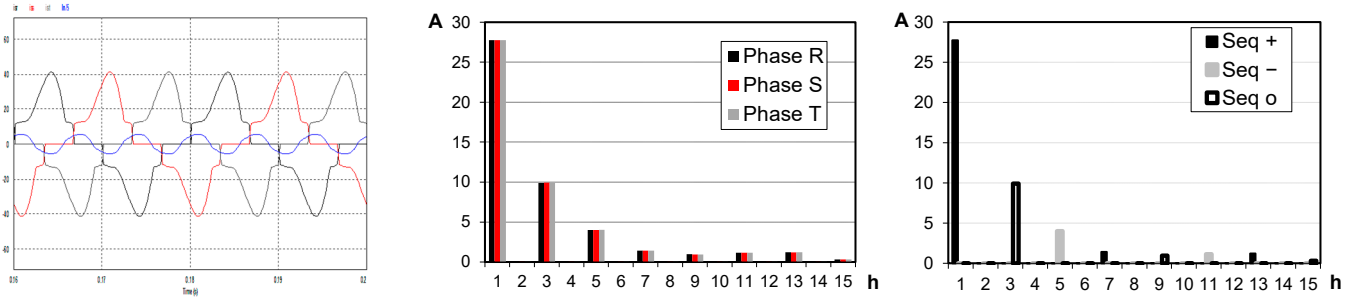

(**a**) (**b**) (**c**)

Figure 9. Case A—(**a**) phase current (phases *R*, *S*, and *T* and neutral); (**b**) harmonic spectrum of phase components; (**c**) harmonic spectrum of symmetric components.

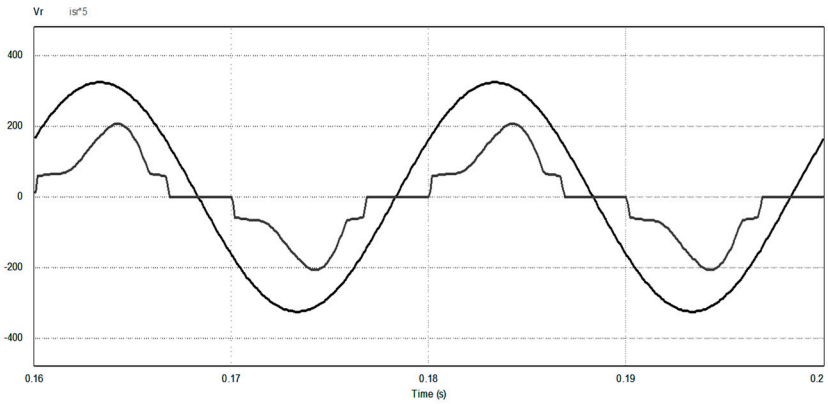

Figure 10. Case A—voltage and current on phase *R*.

B. Balanced, non-linear loads with ShAPF in operation

Figure 11 illustrates the steady-state currents' waveforms on the source side with a three-leg ShAPF connected. On the graph scale, the neutral current was divided five times. The results presented in Figure 11b,c clearly show the performance of the ShAPF, which substantially reduced the harmonic components of the fifth and seventh orders with predominantly sequential distribution in the negative and positive phase sequences, respectively. However, the presence of the third harmonic order was observed, with a strong concentration in the zero-sequence. As expected, in the configuration adopted for the ShAPF with only three legs, the third component could not be compensated. Thus, the residual harmonic distortion was practically due to the presence of this component with an amplitude of 9.7A.

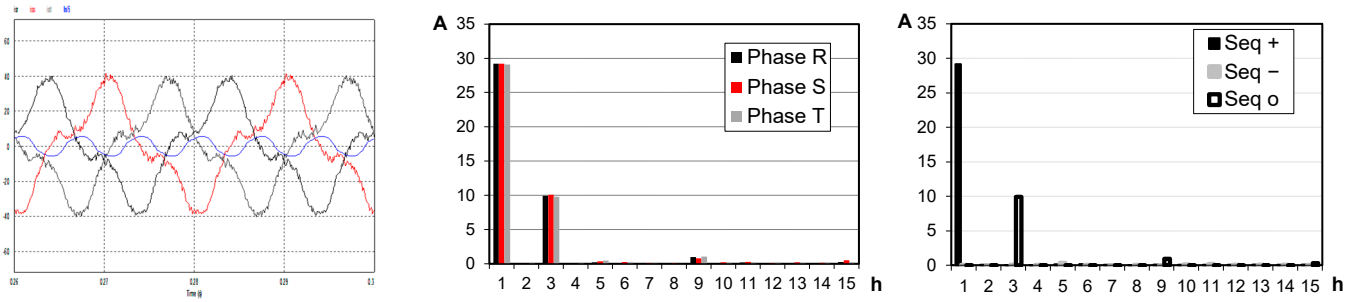

(**a**) (**b**) (**c**)

Figure 11. Case B—(**a**) supply currents (phases *R*, *S*, and *T* and neutral); (**b**) harmonic spectrum of phase components; (**c**) harmonic spectrum of the symmetric components.

Figure 12 shows, for the same phase, the voltage and the respective current on the source side. To facilitate the visualization of the results, in the graphic scale, the phase current was multiplied five times. The power factor obtained in this case was 0.94. This significant improvement in the power factor was due to the reduction of the fifth and seventh harmonic components, compensated by the action of the ShAPF.

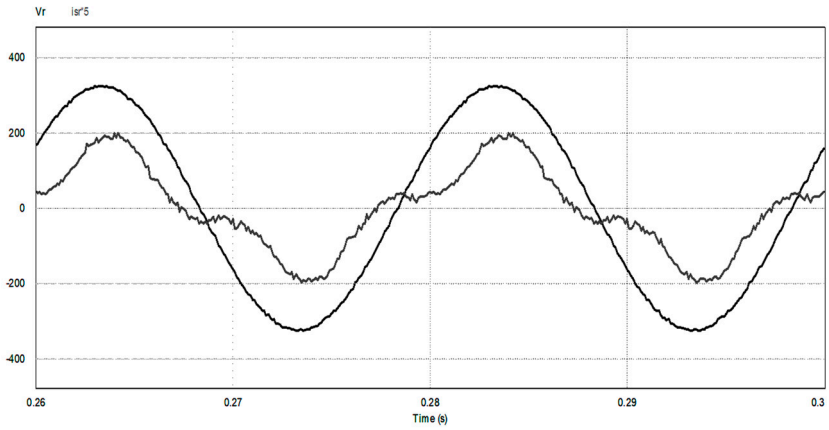

Figure 12. Case B—voltage and current on phase *R*.

C. Balanced, non-linear loads with ShAPF and ZSF in operation

Figure 13a illustrates the steady-state currents' waveforms on the source side with ShAPF and ZSF connected. On the graph scale, the neutral current was divided five times. With the joint action of the ZSF, it was possible to observe a small improvement in the performance of the compensation system. As can be observed in Figure 13c, a small reduction in third-order components was noticed. This fact was due to the confinement, albeit in a precarious way, of a small portion of the zero-sequence components.

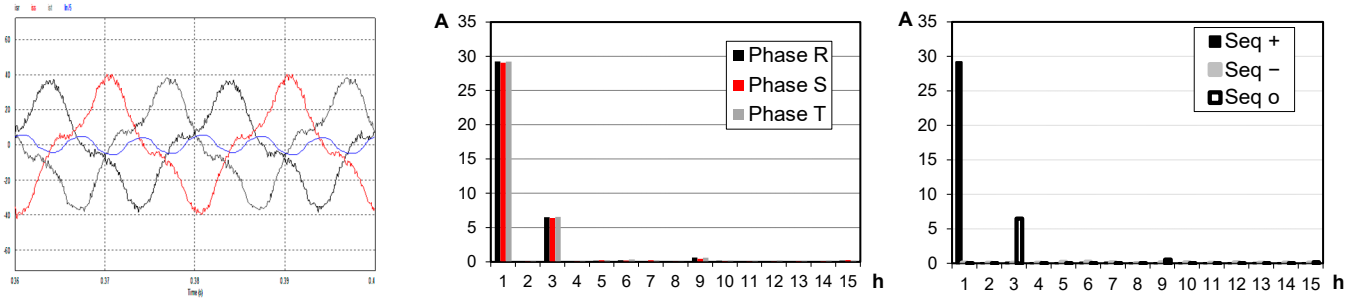

Figure 13. Case C—(**a**) supply currents (phases *R*, *S*, *T*, and neutral). (**b**) Harmonic spectrum of phase components. (**c**) Harmonic spectrum of the symmetric components.

Figure 14 shows, for the same phase, the voltage and the respective current at the source side. To facilitate the visualization of the results, in the graphic scale, the phase current was multiplied five times. The reflection of the harmonic distortion reduction was seen, once again, with the small increase in the power factor to 0.95.

D. Balanced, non-linear loads with ShAPF and ZSS in operation

Figure 15a illustrates the steady-state currents' waveforms on the transformer secondary terminal when considering the HyShAPF, in other words, the complete hybrid compensation system. On the graph scale, the neutral current was divided five times.

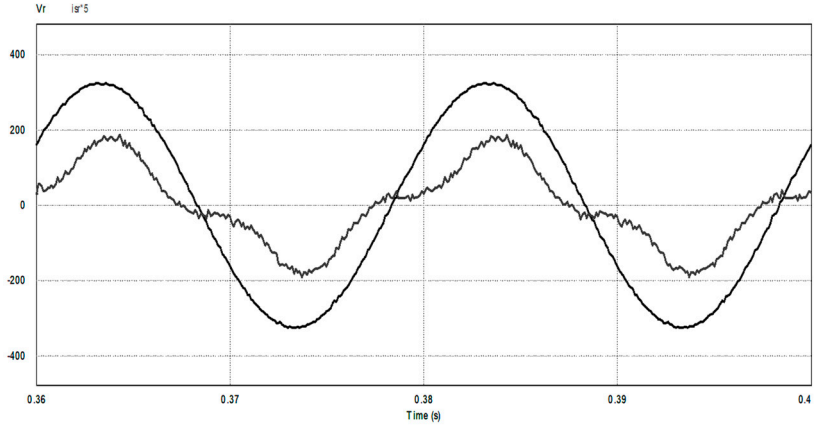

Figure 14. Case C—voltage and current in phase *R*.

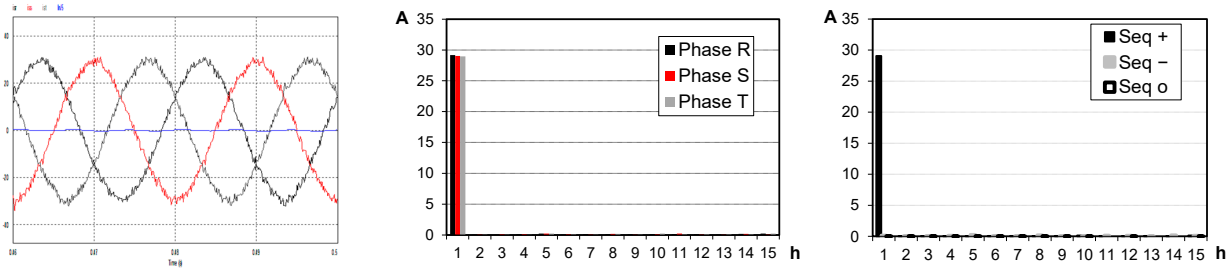

(**a**) (**b**) (**c**)

Figure 15. Case D—(**a**) supply currents (phases *R*, *S*, *T*, and neutral); (**b**) harmonic spectrum of phase components; (**c**) harmonic spectrum of the symmetric components.

As seen, the electromagnetic filter acted as a current divider. Under these conditions, in order for its performance to be maximized, the presented zero-sequence impedance had to have a value substantially lower than the respective impedance of the upstream system in relation to the PCC. Thus, in electrical grids where the ZSS PCC presents high levels of short circuit (similar to in the case of the simulation), it is possible that there will be some difficulty in the design of this device from a constructive point of view.

Under these conditions, the use of an auxiliary device, the ZSB, is recommended [20,27]. This equipment, as previously highlighted, in contrast to the ZSF, is designed in such a way as to present a high zero-sequence impedance and low positive and negative sequence impedance. Therefore, in joint operation, the ZSB (connected in series to the system) can function as an impedance adapter and, thus, maximize the functionality of the ZSF (connected in parallel to the system). Figure 15b,c presents the results for the sequential harmonic components for the operational conditions described. In this case, an expressive reduction of the zero-sequence components was observed, thus, favoring the best performance of the compensation system composed of the ShAPF and the ZSS.

Figure 16 illustrates, for the same phase, the voltage and the respective current at the source side. To facilitate the visualization of the results, in the graphic scale, the phase current was multiplied five times. The power factor obtained in this case was practically unitary since the current harmonic distortion was substantially reduced.

E. Unbalanced, non-linear loads without the action of filters

In order to investigate the capacity of the HyShAPF in operational situations with large load imbalances, some illustrative results are presented below. The unbalanced, non-linear load configuration was defined in one phase, specifically, in one of the single-phase rectifiers with capacitive filter. Figure 17a illustrates the steady-state currents' waveforms on the source side, without the action of filters, which were taken as a reference for subsequent analyses. On the graph scale, the neutral current was divided five times. By analyzing

Figure 17b,c it is possible to verify the unbalanced characteristic of the resulting total load. As expected, the fundamental component presented non-zero values in the three phase sequences. The same was observed for the other sequential components, although the concentration in the respective typical phase sequences was still detected.

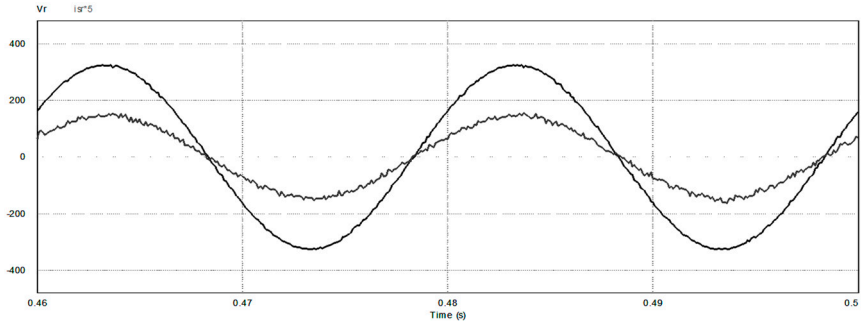

Figure 16. Caso D—voltage and current in phase *R*.

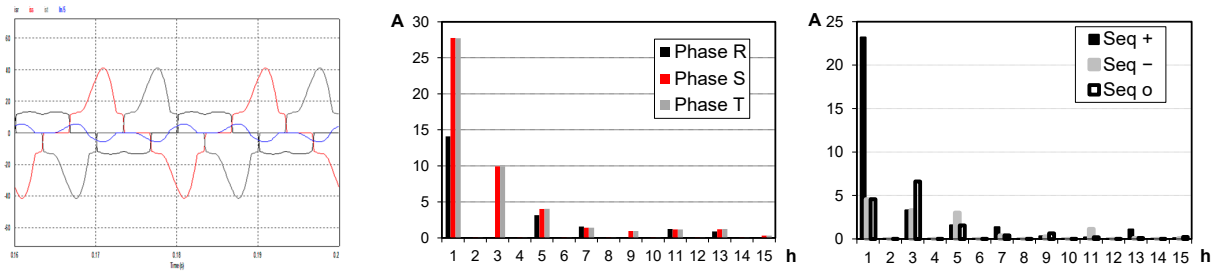

(**a**) (**b**) (**c**)

Figure 17. Case E—(**a**) supply currents (phases *R*, *S*, and *T* and neutral); (**b**) harmonic spectrum of phase components; (**c**) harmonic spectrum of the symmetric components.

F. Unbalanced, non-linear loads only with ShAPF in operation

Figure 18a illustrates the steady-state currents' waveforms on the source side for unbalanced loading under the action of only the three-leg ShAPF. On the graph scale, the neutral current was divided five times. The results indicate the expected action of the ShAPF, which reduced, for example, the levels of the fifth and seventh harmonic components concentrated in negative and positive sequences, respectively, as seen in Figure 18b,c. It is noteworthy that, in this case, due to the imbalance imposed by the asymmetry of the loads, the entire harmonic spectrum concentrated in the zero-sequence remained unchanged in relation to the previous case, including for the fifth and seventh harmonic orders. Naturally, such behavior was predictable as the topology adopted for the ShAPF does not support the compensation of zero-sequence powers. Thus, the imbalance and residual distortions were directly related to the presence of homopolar components in the different harmonic frequencies as well as in the fundamental component.

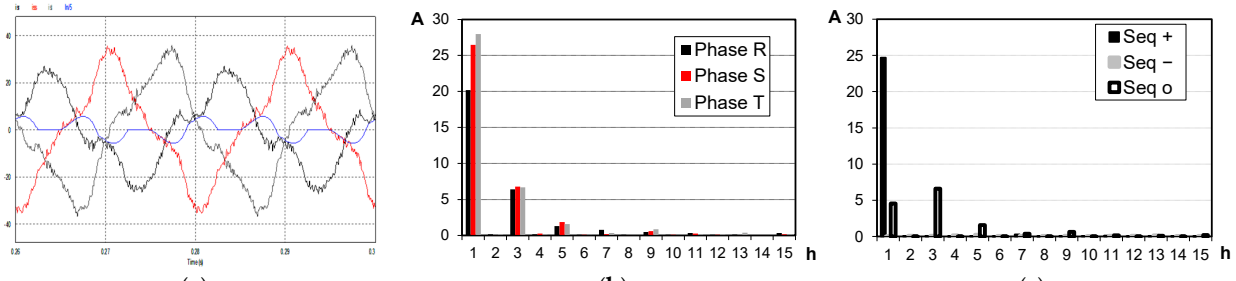

(**a**) (**b**) (**c**)

Figure 18. Case F—(**a**) supply currents (phases *R*, *S*, and *T*, and neutral); (**b**) harmonic spectrum of phase components; (**c**) harmonic spectrum of the symmetric components.

G. *Unbalanced, non-linear loads with HyShAPF in operation*

Figure 19a illustrates the steady-state currents' waveforms on the source side considering the performance of the complete hybrid filter arrangement, the HyShAPF. On the graph scale, the neutral current was divided five times. The performance of the hybrid compensation system was, once again, satisfactorily verified. The combined electromagnetic devices confined the zero-sequence components only between their PCC and the loads, thus, inhibiting their flow through the other paths of the grid, as shown in Figure 19b,c. In this case, there was a significant reduction of all zero-sequence components in the currents coming from the power supply, with a direct benefit to the residual levels of unbalances and harmonic distortions.

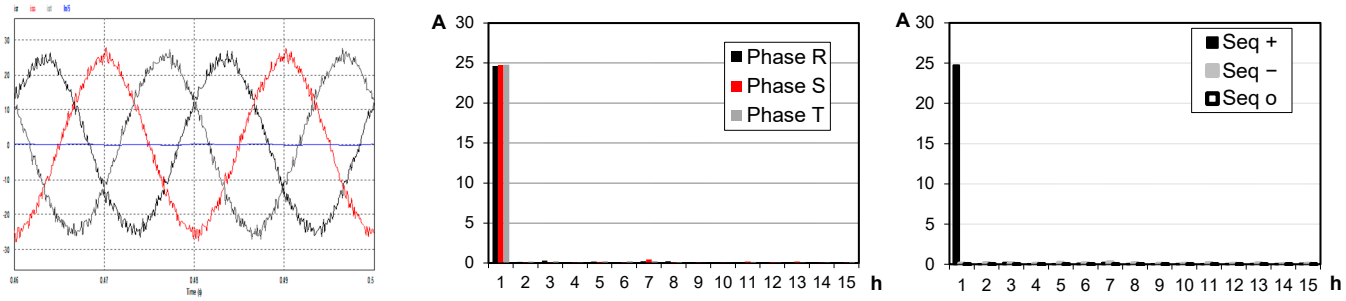

(**a**) (**b**) (**c**)

Figure 19. Case G—(**a**) supply currents (phases *R*, *S*, and *T* and neutral); (**b**) harmonic spectrum of phase components; (**c**) harmonic spectrum of the symmetric components.

H. *Comparing Results*

The overall results presented in Table 2 briefly demonstrate some characteristics of the currents on source side for different arrangements of the compensation system and for the different loading conditions analyzed above (balanced load—BL—and unbalanced load—UL). The effective values of the currents in the three phases, the effective values of the sequential components, the current total harmonic distortions (THD_C), and the residual unbalance factors in the negative (UF-) and zero (UF_0) sequence are presented. For the residual unbalance factors, two versions are particularly presented. The first refers to the unbalance factor classically known as the relation between the rms values of the negative and positive sequence currents. The second, less usual, but particularly important in this evaluation, represents the relationship between the effective values of the zero- and positive sequence components. Considering, therefore, a four-wire system, where, eventually the zero-sequence components may be present, the perfect symmetry between the currents in the lines is guaranteed when the two unbalance factors mentioned are simultaneously zero.

Table 2. Results for different combinations of the hybrid filter arrangement.

Arrangements	Currents (A_rms)			Sequencies (rms)			THD_C (%)			UF (%)	
	R	*S*	*T*	(+)	(-)	(0)	*R*	*S*	*T*	(+)	(0)
BL/without filters	21.2	21.1	21.2	19.7	3.1	7.1	39.9	40	40	0.1	0.1
BL/ShAPF	21.9	21.9	22.0	20.1	0.5	7.1	34.4	34.6	33.6	0.5	0.0
BL/ShAPF + ZSF	21.6	22	21.6	20.8	0.4	6.4	31.7	30.4	31.0	0.6	1.9
BL/ShAPF + ZSF + ZSB	20.6	20.6	20.6	20.6	0.4	0.1	2.7	2.7	2.7	0.1	0.1
UL/without filters	10.4	21.1	21.1	16.7	4.7	5.8	28.8	39.9	40.0	19.7	19.8
UL/ShAPF	15.0	19.4	20.4	17.5	0.5	5.8	33.8	26.1	25.1	0.5	18.6
UL/ShAPF + ZSF + ZSB	17.4	17.3	17.5	17.4	0.4	0.2	3.0	3.7	3.1	0.1	0.7

The comparative results illustrated in Figure 20, generated from the data presented in Table 2, clearly show the importance of electromagnetic devices in reducing the THD_C of supply currents. In the first investigated cases where the single-phase loads operated symmetrically, the harmonic multiples of three, with a strong concentration in the zero-sequence, could not be compensated by the three-leg ShAPF. So, with only the ShAPF acting, the harmonic distortions, although they were significantly reduced, remained, on average, with residual values of around 86% of the original distortion (from 40% to 34.2%). With the introduction of the ZSF, there was an ineffective reduction in residual harmonic distortions of about 8%. However, with the input of the ZSB, which makes up the so-called ZSS, the reduction of harmonic distortion in the supply currents was greater than 90% on average. For load imbalance conditions, the results obtained were also encouraging and clearly show the efficiency of ZSS in confining zero-sequence components, as shown in Figure 21.

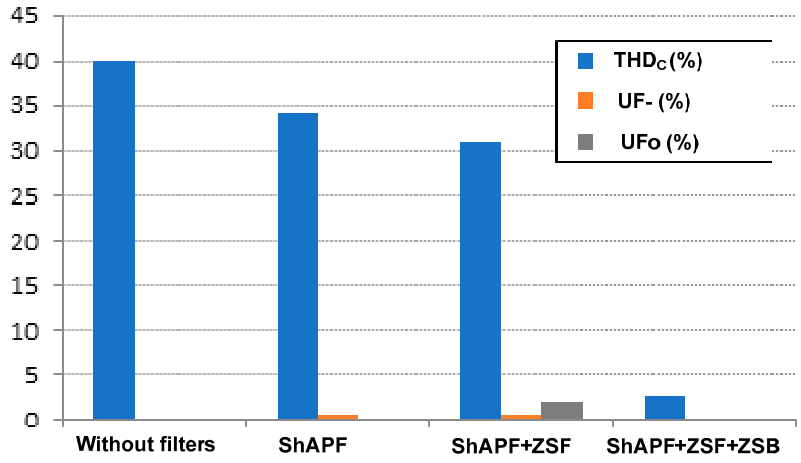

Figure 20. Total harmonic distortions and current unbalance factor with the variation of the filter arrangement with balanced load.

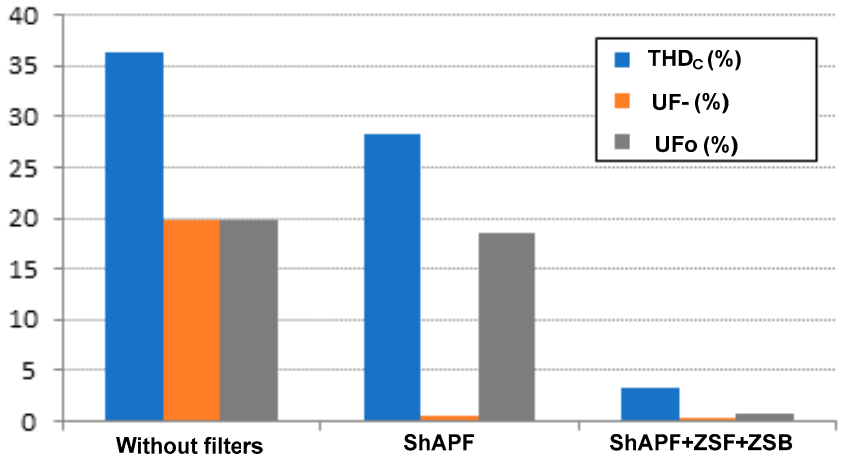

Figure 21. Total harmonic distortions and current unbalance factor with the variation of the filter arrangement with unbalanced load.

The joint action of the ShAPF and the ZSS ensured residual zero-sequence unbalance indices lower than 0.7%, thus, providing a reduction of approximately 96% (from 19.8% to 0.7%) compared to the value obtained only with the ShAPF actuation. In addition, the reduction in the negative sequence unbalance provided by ShAPF was even more effective when it was operated in conjunction with ZSS, and, under these conditions, there was a reduction of about 99.5% (from 19.7% to 0.1%).

4. Experimental Results

In this section, experimental results of the proposed HyShAPF, described in Section 2, consisting of a ZSS and ShAPF, are presented. Initially, a brief explanation of the experimental procedures is presented, including a brief description of the materials and equipment used. Then, with a view to a more enlightening presentation, some tests are described in which the focus was to illustrate the behavior of the system under different operating conditions. With regard to the results obtained from the experiments, only a few specific cases are chosen, the most representative to show the effectiveness of the proposed HyShAPF.

4.1. Experimental Procedures, Materials, and Equipment

The active and passive filtering systems were set up as a platform for the development of the experimental analyses, as illustrated in Figures 22 and 23. The system in Figure 22 was composed of a non-linear load, a ZSS (ZSF and ZSB), a three-wire ShAPF, and three VARIACS. The system in Figure 23 consisted of a four-wire ShAPF, the same non-linear load as illustrated in Figure 23 and the three VARIACS. The new HyShAPF arrangement was evaluated through a comparison between its performance and the performance of the four-wire ShAPF.

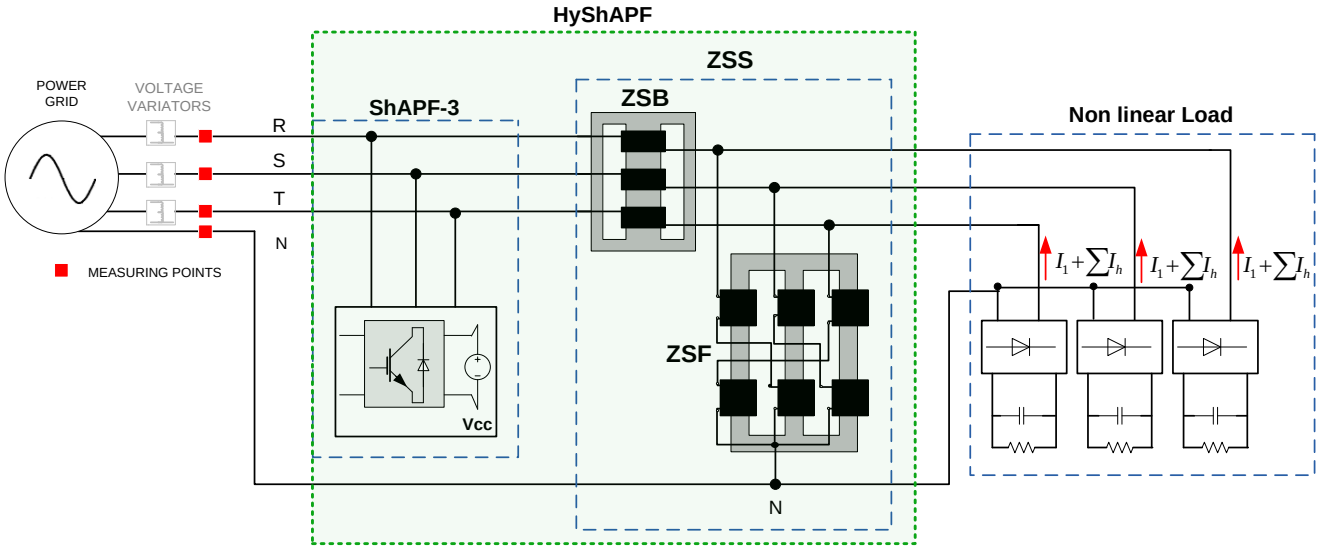

Figure 22. Schematic diagram for experimental studies of the proposed HyShAPF arrangement.

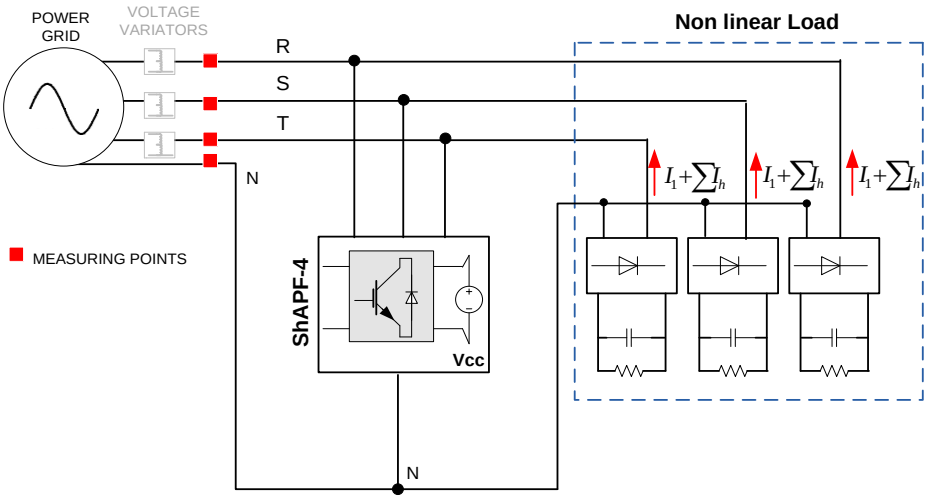

Figure 23. Schematic diagram for experimental studies of the four-wire ShAPF.

The frequency and the lags between the test voltages were determined by the power supply network since the filtering devices and loads were connected directly to the power grid. The data acquisition control and the processing of captured signals were carried out through the Fluke 434 Power Quality Analyzer® and FlukeView® Power Quality Analyzer.

Figure 24 illustrates the general view of the laboratorial set up for the experimental analyses with all the components of the HyShAPF arrangement.

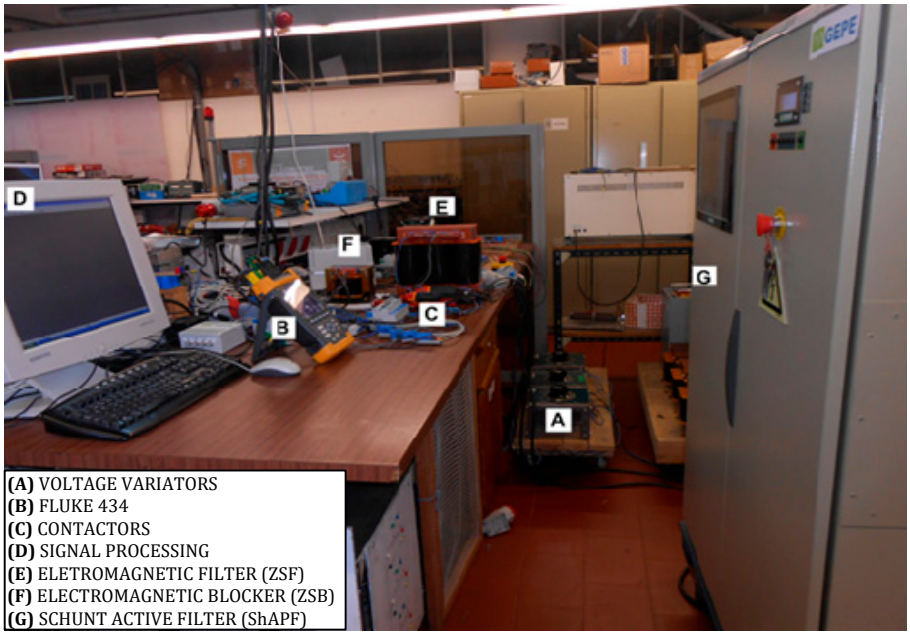

Figure 24. General overview of the workbench used in the experimental tests.

For the composition of the three-phase, non-linear load, an arrangement with a significant concentration of zero-sequence harmonics was chosen but which also generated positive and negative sequence harmonic currents. For this purpose, a non-linear, three-phase load composed of three single-phase rectifiers with capacitive filtering was adopted, feeding variable resistive loads. Figure 25 illustrates the arrangement used for these rectifiers.

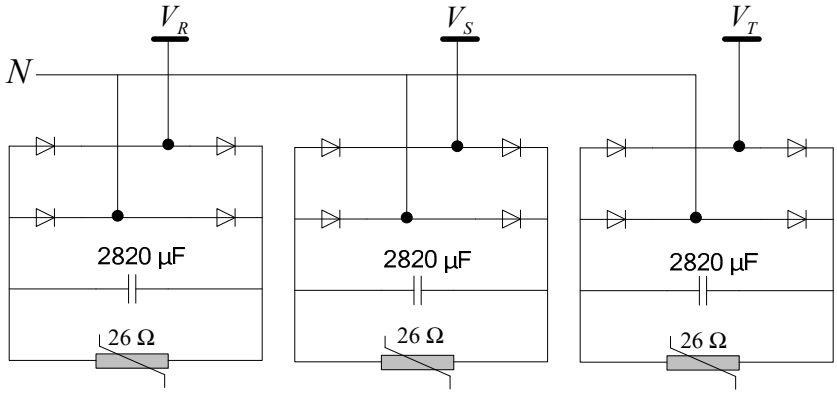

Figure 25. Three-phase, balanced, non-linear load.

For the experimental tests, the prototypes of the ZSF and ZSB, designed according to the criteria established in [20,41], were used. Table 3 contains the nominal data of the prototypes built. The ShAPF used in the experimental tests of this work was the same one presented in [42]. Table 4 presents some of the main parameters of the ShAPF.

Table 3. ZSS main parameters.

Parameter	Value
ZSF nominal power	6.7 kVA
ZSF nominal voltage	230 V
ZSF coil self-inductance	300 mH
ZSF mutual inductance between coils in the same column	0.99
ZSB nominal power	1.1 kVA
ZSB maximum voltage drop	15 V
ZSB coil self-inductance	5 mH
ZSB mutual inductance between coils in the same column	0.99

Table 4. ShAPF parameters [42].

Parameter	Value
Sampling frequency	32 kHz
DC-link capacitor	740 uF
Output inductors	5 mH
Maximum switching frequency	16 kHz

4.2. Functionalities of the Hybrid Filter Arrangement

The analyses presented here were carried out for different arrangements of the system in a steady state, with the main objective of investigating the functionality of the HyShAPF, verifying, through a performance comparison with the four-wire ShAPF, whether the filter arrangement proposed in this thesis presents all the functionalities of a four-wire ShAPF. The operational conditions imposed for the experimental tests are presented in Table 5. To facilitate the descriptions in the figures and tables, abbreviations are used to refer to the three-wire ShAPF (ShAPF-3) and the four-wire ShAPF (ShAPF-4).

Table 5. Selected test cases.

Case	Loads	ZSS	ShAPF-3	ShAPF-4
1	Balanced	OFF	OFF	OFF
2	Balanced	ON	ON	OFF
3	Balanced	OFF	OFF	ON
4	Unbalanced	OFF	OFF	OFF
5	Unbalanced	ON	ON	OFF
6	Unbalanced	OFF	OFF	ON

The results illustrated below are presented by means of waveforms of voltages and currents, including the respective harmonic spectra of phase components and sequential components.

I. Case 1—System without filters with balanced loads

The objective of this case was to observe the harmonics injected by the set of loads in the system without any filtering device.

This topology refers to the operation of the system without any filtering device. To compose the load, three single-phase rectifiers built in a bridge topology were adopted. The load was supplied directly from the power grid. These results were taken as a reference for the comparative effect of the performance of the filtering systems presented in cases 2

and 3, highlighting the waveforms and the harmonic spectrum of the three-phase currents and voltages. Figures 26 and 27 illustrate the waveforms and harmonic distortion levels of voltages and currents in the three-phase system.

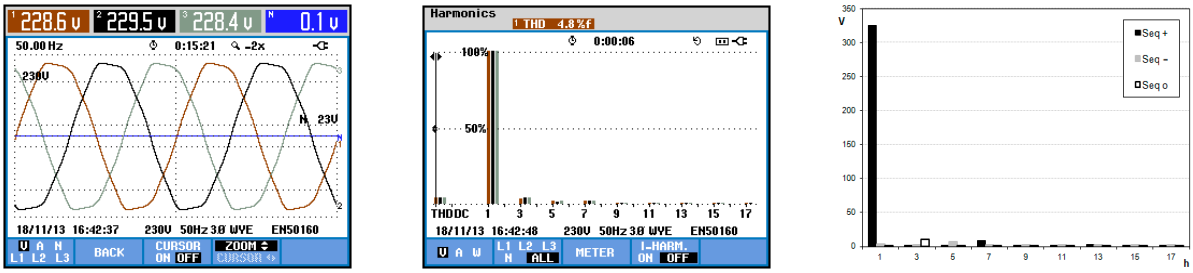

(**a**) (**b**) (**c**)

Figure 26. Case 1—system without filters: (**a**) three-phase voltages; (**b**) harmonic spectrum of the voltages; (**c**) harmonic spectrum of the voltage sequence components (maximum values).

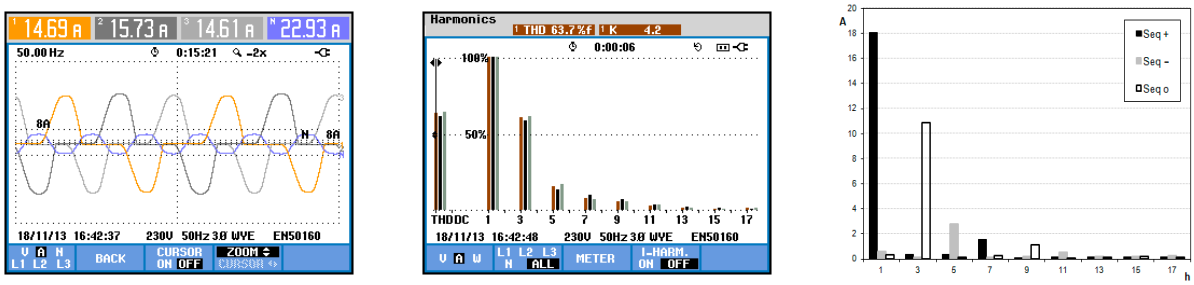

(**a**) (**b**) (**c**)

Figure 27. Case 1—system without filters: (**a**) three-phase currents; (**b**) harmonic spectrum of the currents; (**c**) harmonic spectrum of the current sequence components (maximum values).

The results obtained in the experiment indicated a voltage total harmonic distortion (THD), obtained by the average of the THD in each of the phases, of 4.2%, as shown in Figure 26b,c. The current THD was 63.1% (average of the THD in each of the phases), as shown in Figure 27b,c. As expected, the third harmonic, with strong concentration in the zero-sequence, presented the most relevant amplitude. However, the fifth-, seventh-, and ninth-order harmonics also contributed to the THD. It is noteworthy that the value of the current in the neutral conductor, 22.93 A, exceeded the value of the phase currents. As, in this case, there was no filtering device connected between the source and the load, the active, reactive, and apparent power, as well as the power factor, were identical, whatever the measurement point. The values of active, reactive, and apparent power in the load, as well as the power factor, are shown in Figure 28. The power factor obtained in this case was 0.8 and was fundamentally due to the harmonic distortion generated by the load.

(**a**) (**b**)

Figure 28. Case 1—system without filters: (**a**) source power; (**b**) voltage and current waveforms in phase *S*.

II. Case 2—ZSS and three-wire ShAPF with balanced loads

In this case, the hybrid arrangement of active and passive filters was connected to the system. The schematic diagram for the analysis of case 2 is illustrated in Figure 22. The experimental results obtained for the supply voltages and currents with the ZSS and the three-wire ShAPF are illustrated in Figures 29 and 30.

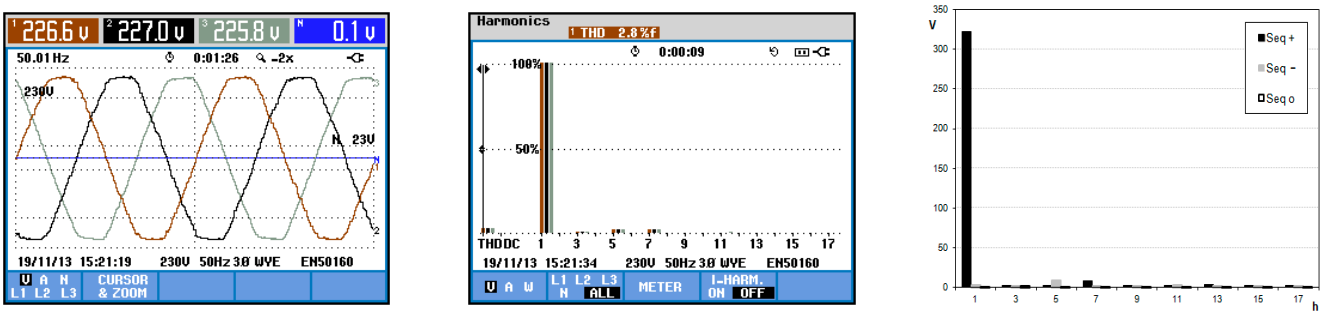

(**a**) (**b**) (**c**)

Figure 29. Case 2—ZSS and three-wire ShAPF operating with balanced loads: (**a**) three-phase voltages; (**b**) harmonic spectrum of the voltages; (**c**) harmonic spectrum of the voltage sequence components (maximum values).

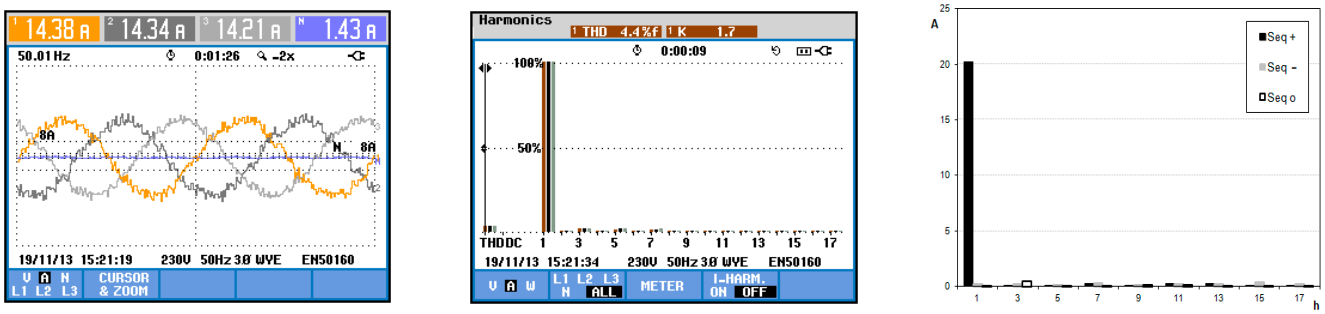

(**a**) (**b**) (**c**)

Figure 30. Case 2—ZSS and three-wire ShAPF operating with balanced loads: (**a**) three-phase currents; (**b**) harmonic spectrum of the currents; (**c**) harmonic spectrum of the current sequence components (maximum values).

The results presented in Figure 30 show a drastic reduction of the third-order current components. This fact was due to the good relationship between the zero-sequence impedance of the system in the PCC and the impedance of the ZSS, favoring the deviation of the zero-sequence current component. As expected, this behavior was provided by the presence of the ZSB in series with the power grid. Another outstanding factor in the joint operation of the ZSS was the significant reduction in the neutral conductor current, going from 22.93 A (case 1) to 1.43 A. It was effective and satisfactory since the operation of the ZSS, together with the three-wire ShAPF, implemented the functionalities of a four-wire ShAPF, which filters all harmonic orders.

The power factor obtained in this case was 0.99, as presented in Figure 31a. This improvement was due to the filtering system in question, which left the voltage and current practically in phase, as seen in Figure 31b.

Figure 32 illustrates the waveforms of the currents that passed through the ZSS and their respective harmonic spectra, where its homopolar characteristic was verified and had predominant frequency in the third harmonic.

(**a**) (**b**)

Figure 31. Case 2—ZSS and three-wire ShAPF operating with balanced loads: (**a**) source power; (**b**) voltage and current waveforms in phase *S*..

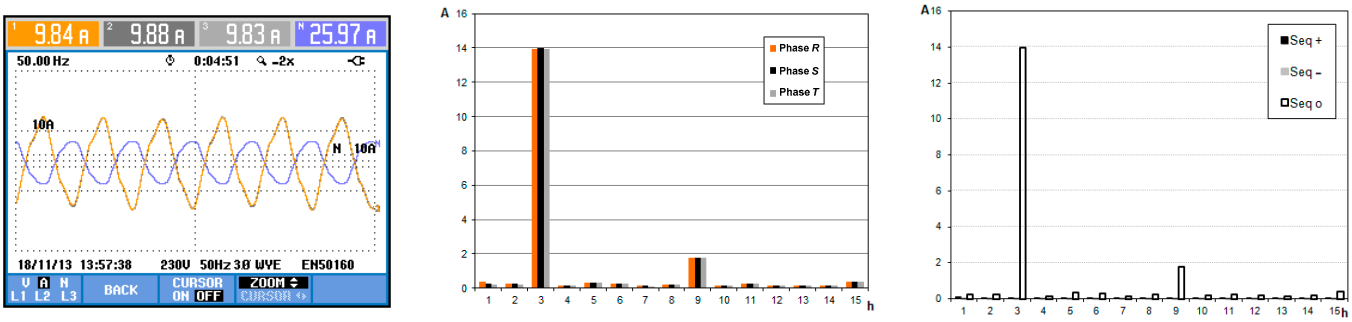

(**a**) (**b**) (**c**)

Figure 32. Measurements in the ZSF: (**a**) three-phase currents; (**b**) harmonic spectrum of the currents; (**c**) harmonic spectrum of the current sequence components (maximum values).

As expected, the ZSS provided a low-impedance path for the zero-sequence harmonics to flow along. Thus, from the point of view of harmonic mitigation, this meant that, under balanced operating conditions, all triplen harmonics were filtered by this device. On the other hand, a high positive sequence impedance was foreseen in the design of the ZSS, which also imposed some positive and/or negative sequence residual component circulating by the device.

III. Case 3—Four-wire ShAPF operating with balanced loads

Aiming to carry out a comparative analysis between the performances of the HyShAPF and a four-wire ShAPF, the system in Figure 23 was assembled. In this case, the harmonic filtering was solely in charge of the four-wire ShAPF. Figures 33 and 34 illustrate the results for three-phase voltages and currents.

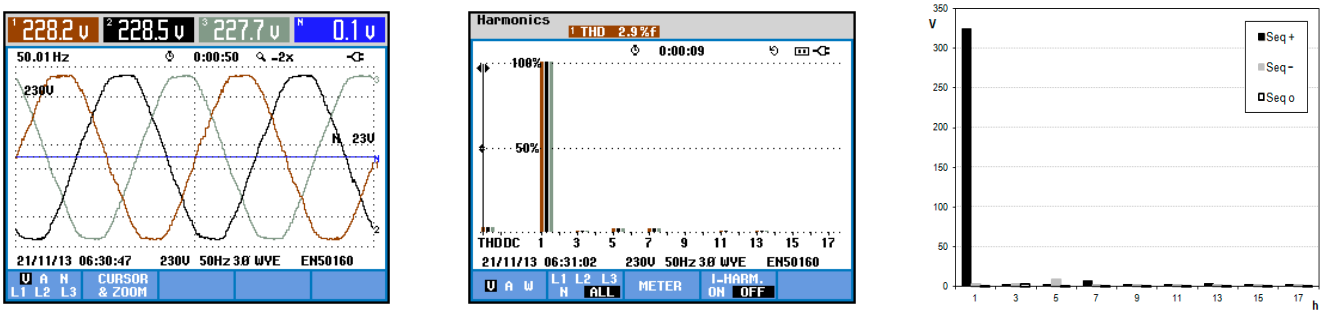

(**a**) (**b**) (**c**)

Figure 33. Case 3—Four-wire ShAPF operating with balanced loads: (**a**) three-phase voltages; (**b**) harmonic spectrum of the voltages; (**c**) harmonic spectrum of the voltage sequence components (maximum values).

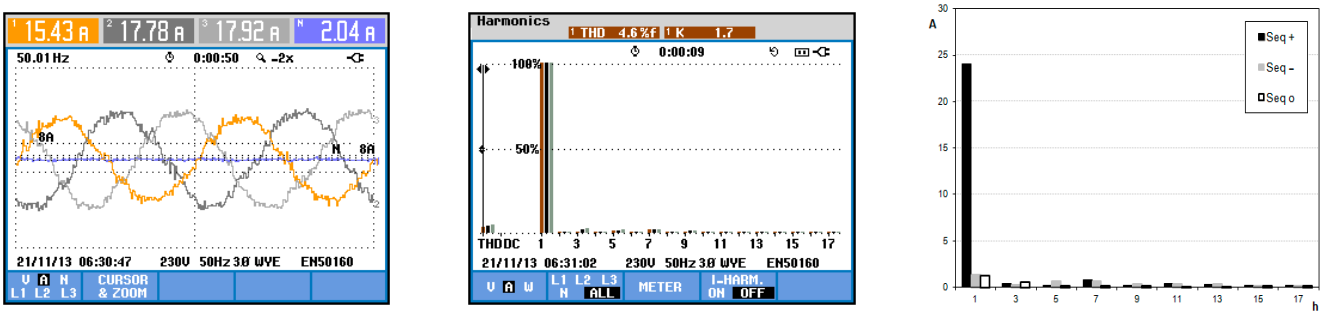

(**a**) (**b**) (**c**)

Figure 34. Case 3—four-wire ShAPF operating with balanced loads: (**a**) three-phase currents; (**b**) harmonic spectrum of the currents; (**c**) harmonic spectrum of the current sequence components (maximum values).

Observing Figure 33b,c, one can see a decrease in voltage distortion, which was 4.2% in case 1, and, after harmonic compensation, it became 2.9%. As expected, the performance of the four-wire ShAPF showed a substantial reduction in the THD distortion in the system, acting in the compensation of all current harmonic orders previously observed in case 1. Another important point of analysis where the effectiveness of the four-wire ShAPF was noted was the value of the current in the neutral conductor, which was minimized from 22.93 A (case 1) to 2.04 A.

The source power data, as well as the voltage and current waveforms in the phase *S*, for case 3 are presented in Figure 35.

(**a**) (**b**)

Figure 35. Case 3—four-wire ShAPF operating with balanced voltages and balanced loads: (**a**) source power; (**b**) voltage and current waveforms in phase *S*.

The power factor obtained in this case was also 0.99. It was observed that, in situations of balanced voltages and balanced loads, the performance of the HyShAPF proposed in this work was very similar to that of the four-wire ShAPF. This fact reveals that, under the tested conditions, the ZSS operating in conjunction with the three-wire ShAPF had the same functionalities as a four-wire ShAPF. Table 6 presents a summary of the results presented in cases 1, 2, and 3.

Table 6. Comparison of results for cases 1, 2, and 3.

	Case 1: Without Filters	**Case 2: With ZSS and ShAPF-3**	**Case 3: With ShAPF-4**
Voltages THD (%)	4.2	3.0	2.9
Current THD (%)	63.1	3.6	4.2
Neutral Current (A)	22.93	1.43	2.04
PF	0.8	0.99	0.99

IV. Case 4—System without filters with unbalanced loads

The objective of this case was to investigate the performance and capacity of the HyShAPF in a situation of load imbalance. For this case, the unbalanced, non-linear load configuration was defined by changing the parameters of one of the single-phase rectifiers. The new load configuration is shown in Figure 36.

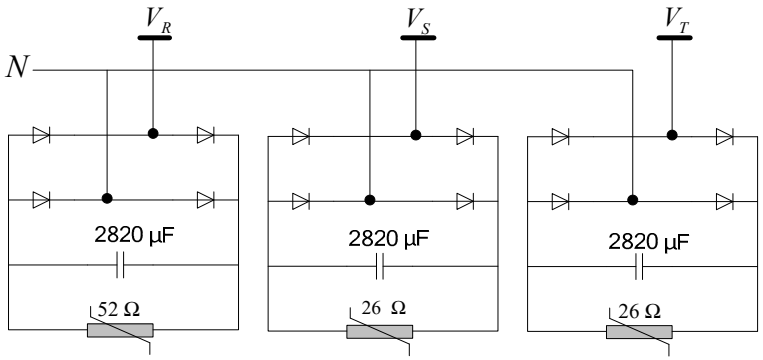

Figure 36. Three-phase, unbalanced, non-linear load.

Figures 37 and 38 illustrate the waveforms of the three-phase supply voltages and currents without the action of the filters. This case was taken as a reference for the analyses of cases 5 and 6.

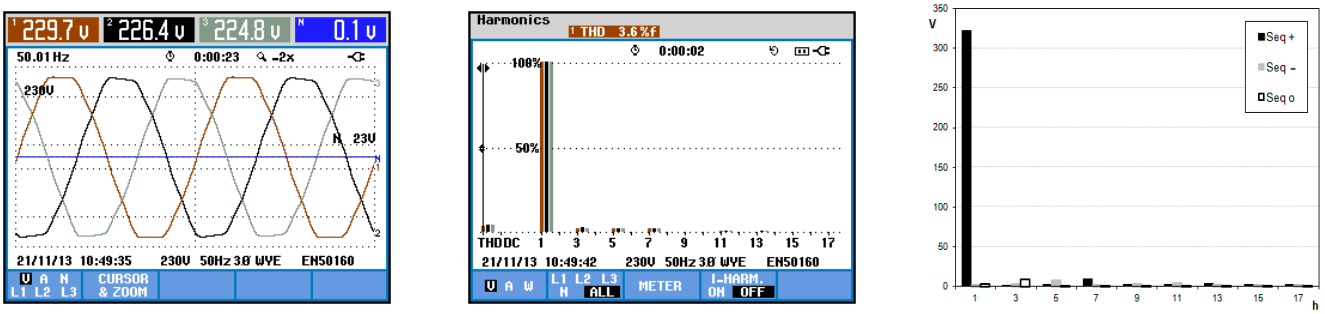

(**a**) (**b**) (**c**)

Figure 37. Without filters with unbalanced loads: (**a**) three-phase voltages; (**b**) harmonic spectrum of the voltages; (**c**) harmonic spectrum of the voltage sequence components (maximum values).

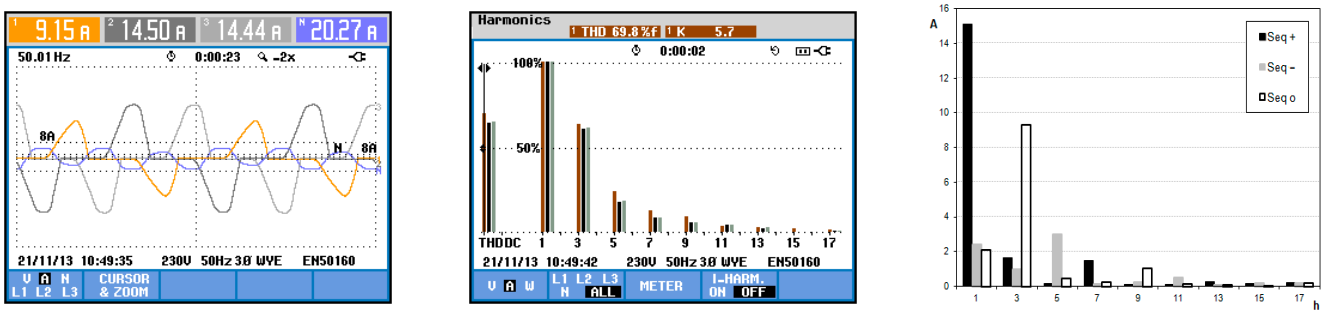

(**a**) (**b**) (**c**)

Figure 38. Case 4—without filters with unbalanced loads: (**a**) three-phase currents; (**b**) harmonic spectrum of the currents; (**c**) harmonic spectrum of the current sequence components (maximum values).

Analyzing the voltages in the power grid in Figure 37, without the filters acting, one can see an imbalance in the voltages caused by the imbalance imposed on the load. The average voltage THD was 4.1%. By analyzing the three-phase currents, illustrated in

Figure 38a, it is possible to verify the unbalanced characteristic of the load. The same can be observed in the harmonic spectrum of the currents and harmonic spectrum of the current sequence components, which were also not ideally distributed, as seen in Figure 38b,c.

The values of the power factor and the active, reactive, and apparent power in the load are shown in Figure 39a. In this case, the power factor was 0.8 and was mainly due to the harmonic distortion caused by the load. Figure 39b illustrates the voltage and current in phase *S*.

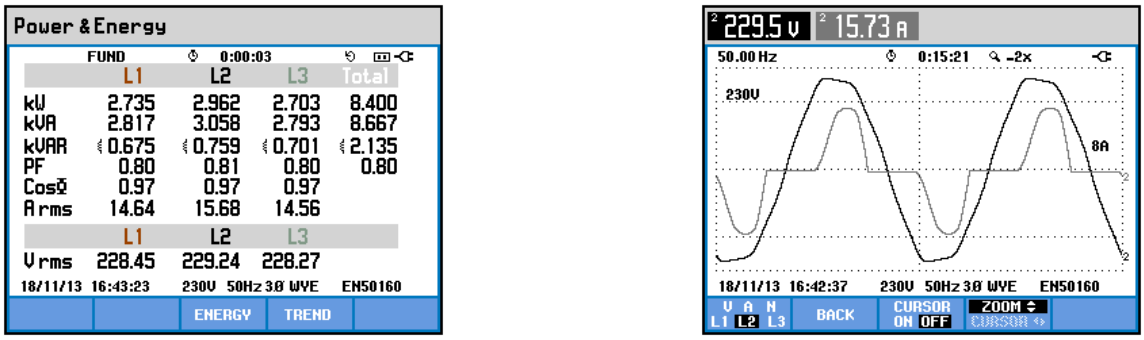

(**a**) (**b**)

Figure 39. Case 4—without filters with unbalanced loads: (**a**) source power; (**b**) voltage and current waveforms in phase *S*.

V. Case 5—ZSS and three-wire ShAPF operating with unbalanced loads

This case proposed the analysis of the system with unbalanced, non-linear loads under the action of the ZSS operating in conjunction with the three-wire ShAPF. The experimental set up was similar to the one illustrated in Figure 24, in which all the system components were connected directly to the power grid. The results obtained are shown in Figures 40 and 41.

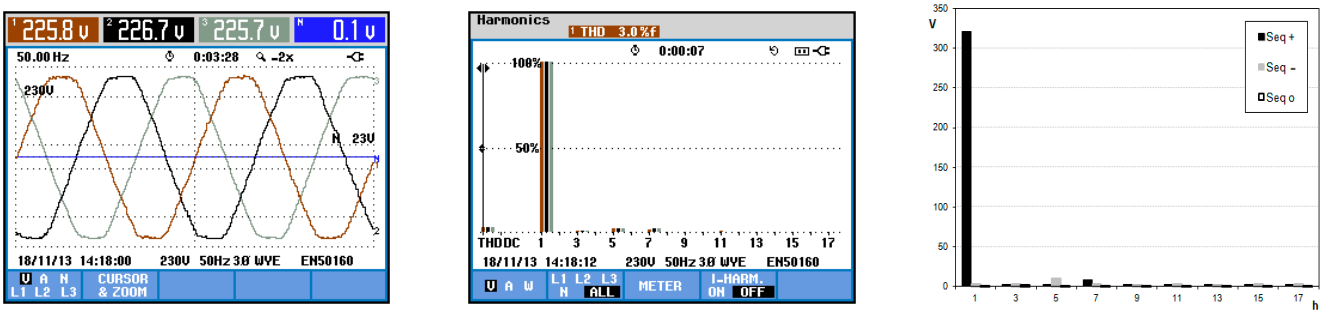

(**a**) (**b**) (**c**)

Figure 40. Case 5—ZSS and three-wire ShAPF operating with unbalanced loads: (**a**) three-phase voltages; (**b**) harmonic spectrum of the voltages; (**c**) harmonic spectrum of the voltage sequence components (maximum values).

The HyShAPF again presented a good performance. Observing Figure 40a, it can be seen that the imbalances previously noticed in the system voltages were reduced. Figure 40b,c shows a minimization of the voltage THD. The three-wire ShAPF acted directly on the compensation of the positive and negative sequence harmonic currents, and the ZSS promoted the considerable confinement of the zero-sequence harmonics between the installation and the non-linear load.

There was, therefore, a relevant reduction of the third and ninth harmonics, shown in Figure 41, with direct benefit to the values of imbalance and THD. Another important factor observed was that, under the action of the filtering devices, the current imbalances seen in the load were practically eliminated in the measurements made at the source.

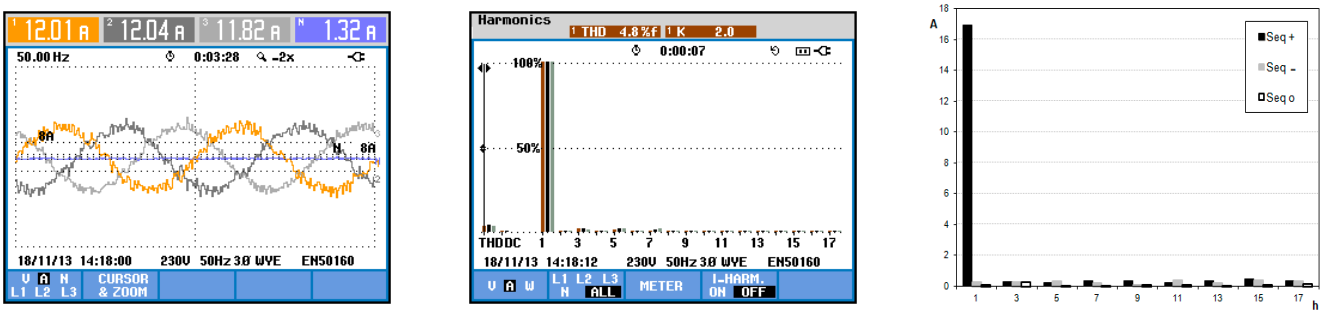

(**a**) (**b**) (**c**)

Figure 41. Case 5—ZSS and three-wire ShAPF operating with unbalanced loads: (**a**) three-phase currents; (**b**) harmonic spectrum of the currents; (**c**) harmonic spectrum of the current sequence components (maximum values).

The values of the active, reactive, and apparent power, as well as the power factor in the source, are shown in Figure 42a. The voltage and current waveforms in phase *S* are shown in Figure 42b. In this situation, the power factor obtained was 0.98. The improvement presented in the power factor was due to the performance of the harmonic filtering. As observed in case 2, the voltage and current were practically in phase.

(**a**) (**b**)

Figure 42. Case 5—ZSS and three-wire ShAPF operating with unbalanced loads: (**a**) source power; (**b**) voltage and current waveforms in phase *S*.

The waveforms of the currents through the ZSF and the harmonic spectra are shown in Figure 43, where its typical and homopolar characteristic is once again verified.

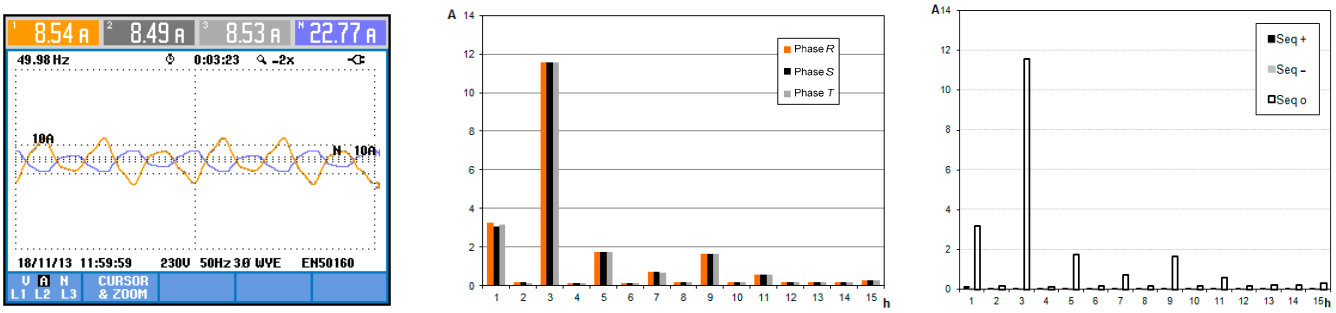

(**a**) (**b**) (**c**)

Figure 43. Measurements in the ZSF: (**a**) three-phase currents; (**b**) harmonic spectrum of the currents; (**c**) harmonic spectrum of the current sequence components (maximum values).

The harmonic spectra in Figure 43 confirm the current imbalances imposed in this case, where it can be seen that there were zero-sequence components not only in triplen harmonics, but also in the fundamental, fifth, and seventh orders. This fact recalls that,

in the sizing process of electromagnetic devices, a possible overload on them due to the fundamental component and other harmonics with homopolar components must be considered. It is worth mentioning, therefore, that the ZSS works as a zero-sequence filter and blocker, and, therefore, regardless of the considered harmonic order, most of the zero-sequence current is conducted by the ZSF.

VI. Case 6—Four-wire ShAPF operating with unbalanced loads

With the aim of carrying out a comparative analysis between the performances of the HyShAPF and the four-wire ShAPF, a system with load imbalance similar to that shown in Figure 36 was implemented. Figures 44 and 45 show the results for the three-phase voltages and currents measured at the source.

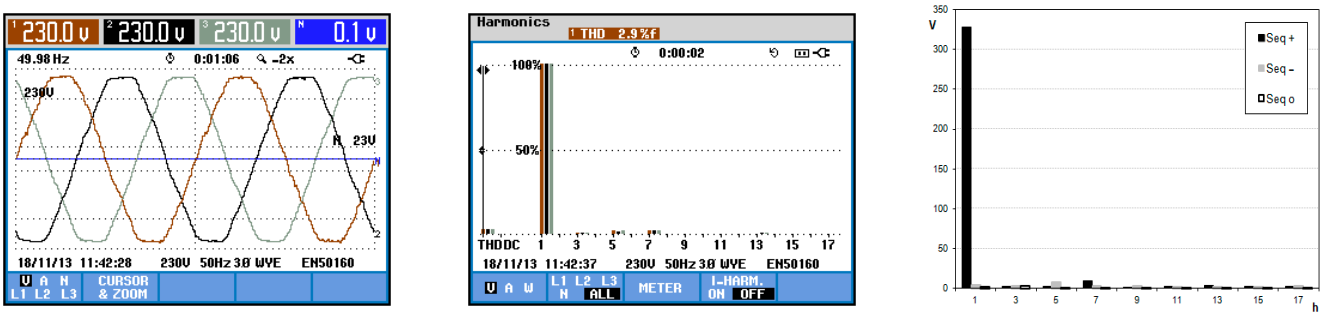

(**a**) (**b**) (**c**)

Figure 44. Case 6—four-wire ShAPF operating with unbalanced loads: (**a**) three-phase voltages; (**b**) harmonic spectrum of the voltages; (**c**) harmonic spectrum of the voltage sequence components (maximum values).

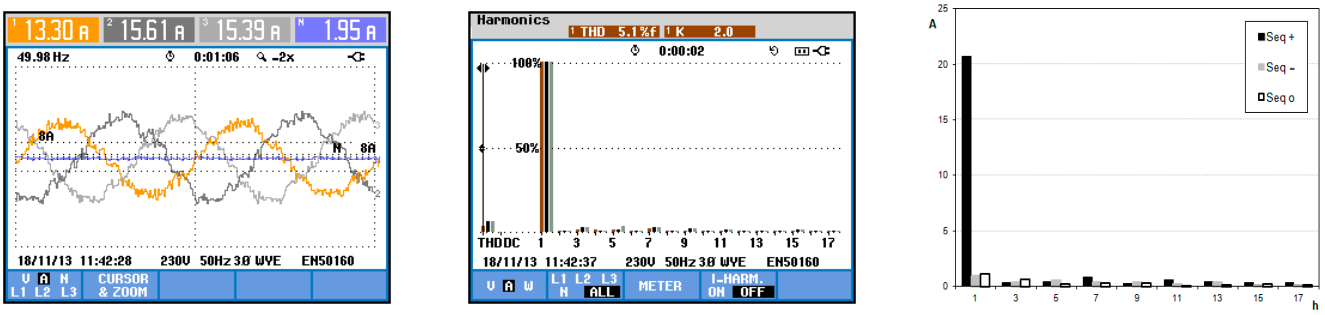

(**a**) (**b**) (**c**)

Figure 45. Case 6—four-wire ShAPF operating with unbalanced loads: (**a**) three-phase currents; (**b**) harmonic spectrum of the currents; (**c**) harmonic spectrum of the current sequence components (maximum values).

With the operation of the four-wire ShAPF, the three-phase voltages at the source were completely balanced, as seen in Figure 44a. There was also a reduction in voltage harmonic levels, with the average voltage THD being 2.9%. Figure 44 shows that, after the operation of the four-wire ShAPF, the total current THD in the system was expressively reduced, falling from 66.3% (case 4) to 5.4%. Another favorable point in the performance of this device was the reduction of the current flowing through the neutral conductor, which was minimized from 20.93 A (case 4) to 1.95 A.

The power at the source, as well as the voltage and current at the phase *S*, is shown in Figure 46.

The power factor measured in this case was unitary. In this situation, with unbalanced loads, the HyShAPF proposed in this work had a very similar performance to the four-wire ShAPF. This fact reveals that, in a situation of load imbalance, the ZSS, operating

in conjunction with the three-wire ShAPF, has practically the same functionalities as a four-wire ShAPF. Table 7 presents a summary of the results presented in cases 4, 5, and 6.

(**a**) (**b**)

Figure 46. Case 6—four-wire ShAPF operating with unbalanced loads: (**a**) source power; (**b**) voltage and current waveforms in phase *S*.

Table 7. Comparison of results for cases 4, 5, and 6.

	Case 4: Without Filters	**Case 5: With ZSS and ShAPF-3**	**Case 6: With ShAPF-4**
Voltages THD (%)	4.1	2.9	3.0
Current THD (%)	66.3	3.7	5.4
Neutral Current (A)	20.27	1.32	1.95
PF	0.8	0.98	1

5. Conclusions

From a technical point of view, the expectations of this research were directed towards results that implement all the functionalities of a four-leg ShAPF through a proposed hybrid arrangement. In this sense, the use of a three-leg ShAPF was proposed, combined with electromagnetic arrangements destined for the confinement of homopolar components, whether these are caused by unbalances in the fundamental frequency or by concentration of harmonic components.

Section 3 of this paper approached the simulation validation, in steady state and transient regimes, of the combined operation of the three-leg ShAPF and the ZSS (parallel filter and series blocker) and confirmed that they perfectly met the assumptions.

As a result, Section 4, the experimental results, presented tests from comparative scenarios, contemplating different arrangements for the filtering system. In addition, experiments that occurred in the form of changes of non-linear loads were analyzed. Among the cases analyzed, only the most enlightening with regard to the understanding of the main phenomena involved in the filtering process and the central objective of this research were exposed. Regarding the performance of the three-leg ShAPF operating in combination with the ZSS, the results indicated the desired performance, since the HyShAPF presented the same functionalities as a four-leg ShAPF, improving effectively the harmonic distortions of currents and voltages and, clearly, the power factor of the system. The performance of the models can, therefore, be considered effective in view of the reliability of the tangible results within the accuracy class of the measurement, data acquisition, and signal-processing equipment. The proposed filter topology has a very high potential for upgrading existing three-leg ShAPFs, the standard topology from manufacturers, to four-wire installations. For new installations, the four-leg ShAPF, a more expensive solution than the standard one, could be a solution to consider.

Author Contributions: Conceptualization, S.F., L.C.O. and J.L.A.; methodology, S.F., P.O., L.C.O. and J.L.A.; software, S.F., P.O., B.E. and J.G.P.; validation, S.F., P.O., B.E. and J.G.P.; investigation, S.F., P.O., B.E., J.G.P., L.C.O. and J.L.A.; resources, J.L.A.; writing—original draft preparation, S.F., P.O., B.E., J.G.P., L.C.O. and J.L.A.; writing—review and editing, S.F., P.O., B.E., J.G.P., L.C.O. and J.L.A.; supervision, L.C.O. and J.L.A. All authors have read and agreed to the published version of the manuscript.

Funding: This research was funded by FCT—Fundação para a Ciência e Tecnologia grant number UIDB/00319/2020.

Data Availability Statement: Data sharing is not applicable to this article.

Acknowledgments: The authors acknowledge the support by CNPq—National Council for Scientific and Technological Development and CAPES—Coordination for the Improvement of Higher Education Personnel. This work was supported by FCT—Fundação para a Ciência e Tecnologia within the R&D Units Project Scope: UIDB/00319/2020.

Conflicts of Interest: The authors declare no conflict of interest.

References

1. Zhang, C.; Xu, Y.; Dong, Z.Y.; Yang, L.F. Multitimescale Coordinated Adaptive Robust Operation for Industrial Multienergy Microgrids With Load Allocation. *IEEE Trans. Ind. Inform.* **2020**, *16*, 3051–3063. [CrossRef]
2. Mohagheghi, S.; Raji, N. Dynamic Demand Response: A Solution for Improved Energy Efficiency for Industrial Customers. *IEEE Ind. Appl. Mag.* **2015**, *21*, 54–62. [CrossRef]
3. Jiang, Z.; Hao, R.; Ai, Q.; Yu, Z.; Xiao, F. Extended multi-energy demand response scheme for industrial integrated energy system. *IET Gen. Transm. Distri.* **2018**, *12*, 3186–3192. [CrossRef]
4. Liang, X. A New Composite Load Model Structure for Industrial Facilities. *IEEE Trans. Ind. Appl.* **2016**, *52*, 4601–4609. [CrossRef]
5. Miranian, A.; Rouzbehi, K. Nonlinear Power System Load Identification Using Local Model Networks. *IEEE Trans. Power Syst.* **2013**, *28*, 2872–2881. [CrossRef]
6. Qu, X.; Li, X.; Song, J.; He, C. An Extended Composite Load Model Taking Account of Distribution Network. *IEEE Trans. Power Syst.* **2018**, *33*, 7317–7320. [CrossRef]
7. IEEE Task Force on Load Representation for Dynamic Performance, Load Representation for Dynamic Performance Analysis. *IEEE Trans. Power Syst.* **1993**, *8*, 472–482.
8. Milanović, J.V.; Yamashita, K.; Villanueva, S.M.; Djokić, S.Z.; Korunović, L.M. International Industry Practice on Power System Load Modeling. *IEEE Trans. Power Syst.* **2013**, *28*, 3038–3046. [CrossRef]
9. Kumar, D.; Zane, F. Harmonic Analysis of Grid Connected Power Electronic Systems in Low Voltage Distribution Networks. *IEEE J. Emerg. Sel. Top. Power Electron.* **2016**, *4*, 70–79. [CrossRef]
10. Sharma, H.; Rylander, M.; Dorr, D. Grid Impacts Due to Increased Penetration of Newer Harmonic Sources. *IEEE Trans. Ind. Appl.* **2016**, *52*, 99–104. [CrossRef]
11. Leite, M.C.C.; Vieira, F.A.M.; Silva, V.B.; Fortes, M.Z.; Dias, D.H.N. Harmonic Analysis of a Photovoltaic Systems Connected to Low Voltage Grid. *IEEE Lat. Am. Trans.* **2018**, *16*, 112–117. [CrossRef]
12. Tang, B.; Ma, S.; Lin, S.; Chen, G.; Fu, Y. Harmonic current emission level assessment of residential loads based on impedance-gathering trend. *Int. Trans. Electr. Energy Syst.* **2017**, 1–13. [CrossRef]
13. Nassif, A.B.; Yong, J.; Xu, W.; Chung, C.Y. Indices for comparative assessment of the harmonic effect of different home appliances. *Int. Trans. Electr. Energy Syst.* **2013**, *23*, 638–654. [CrossRef]
14. Das, J.C. *Harmonic Generation Effects Propagation and Control*, 1st ed.; CRC Press: New York, NY, USA, 2017; ISBN 9781498745468.
15. IEEE TASK FORCE. Effect of harmonics on equipments. *IEEE Trans. Power Deliv. Piscataway* **1993**, *8*, 672–680. [CrossRef]
16. EUROPEAN STANDARD. *EN 50160: Voltage Characteristics of Electricity Supplied by Public Distribution Systems*; Wroclaw University of Technology: Wroclaw, Poland, 1994; 16p.
17. *IEEE SA 519-1992*; Recommended Practices and Requirements for Harmonic Control in Electrical Power Systems. [S. l.: S.n]; IEEE: New York, NY, USA, 1992; 100p, (Industrial Power Converters Committee). Available online: https://edisciplinas.usp.br/pluginfile.php/1589263/mod_resource/content/1/IEE%20Std%20519-2014.pdf (accessed on 22 January 2023).
18. Pichan, M.; Karimi, M.; Simorgh, H. Improved low-cost sliding mode control of 4-leg inverter for isolated microgrid applications. *Int Trans Electr Energ Syst.* **2018**, *28*, e2642. [CrossRef]
19. Nibouche, M.; Bouchhida, O.; Makhlouf, B. Design, analysis and implementation of real-time harmonics elimination: A generalized approach. *IET Power Electron.* **2014**, *7*, 2424–2436.
20. Freitas, S.C.L.; Oliveira, L.C.O.; Silva Oliveira, P.; Exposto, B.; Oliveira Pinto, J.G.; Afonso, J.L. Modeling, design, and experimental test of a zero-sequence current electromagnetic suppressor. *Int. Trans. Electr. Energy Syst.* **2020**, *30*. [CrossRef]
21. Sousa, T.J.C.; Monteiro, V.; Afonso, J.A. Selective Harmonic Measurement and Compensation Using Smart Inverters in a Microgrid with Distributed Generation. In Proceedings of the 2018 IEEE 16th International Conference on Industrial Informatics (INDIN), Porto, Portugal, 18–20 July 2018; pp. 439–444. [CrossRef]

22. Monteiro, L.F.C.; Aredes, M.; Couto, C.; Afonso, J.L. Control algorithms for a unified power quality conditioner based on three-level converters. *Int. Trans. Electr. Energy Syst.* **2014**, *25*, 2394–2411. [CrossRef]
23. Jou, B.H.L.; Wu, J.C.; Wu, K.D.; Chiang, W.J.; Chen, Y.H. Analysis of Zig-Zag Transformer Applying in the Three-Phase Four-Wire Distribution Power System. *IEEE Trans. Power Deliv.* **2005**, *20*, 1168–1173. [CrossRef]
24. Schoene, J.; Walling, R.; Bo, Y.; Niemann, B.; Zheglov, V.; Guinn, D.; Peele, S.; Grappe, J.; Zavadil, B.; Freeman, L. Analysis and mitigation of excessive zero-sequence harmonic currents in distribution systems. In Proceedings of the Transmission and Distribution Conference and Exposition (T&D) IEEE PES, Orlando, FL, USA, 7–10 May 2012; pp. 1–6. [CrossRef]
25. Rahmani, S.; Hamadi, A.; Al-Haddad, K.; Dessaint, L.A. A Combination of Shunt Hybrid Power Filter and Thyristor-Controlled Reactor for Power Quality. *IEEE Trans. Ind. Electron.* **2014**, *61*, 2152–2164. [CrossRef]
26. Bosch, S.; Staiger, J.; Steinhart, H. Predictive Current Control for an Active Power Filter With LCL-Filter. *IEEE Trans. Ind. Electron.* **2018**, *65*, 4943–4952. [CrossRef]
27. Oliveira, J.C.; Oliveira, L.C.O.; Belchior, F.N.; Oliveira, R.N.; Barbosa, J.A., Jr. Frequency domain model for zero-sequence electromagnetic harmonic filter performance analysis. *Int. Trans. Electr. Energy Syst.* **2014**, 1–15. [CrossRef]
28. Oliveira, L.C.O.; Oliveira, R.N.; Souza, J.B.; Freitas, S.C.L. Electromagnetic Zero-Sequence Harmonics Blocker: Modeling and Experimental Analysis. *J. Energy Power Eng.* **2014**, *8*, 1425–1431.
29. Maher, M.; Abdel Aleem, S.H.E.; Ibrahim, A.M.; El-Shahat, A. Novel Mathematical Design of Triple-Tuned Filters for Harmonics Distortion Mitigation. *Energies* **2023**, *16*, 39. [CrossRef]
30. Sufyan, A.; Jamil, M.; Ghafoor, S.; Awais, Q.; Ahmad, H.A.; Khan, A.A.; Abouobaida, H. A Robust Nonlinear Sliding Mode Controller for a Three-Phase Grid-Connected Inverter with an LCL Filter. *Energies* **2022**, *15*, 9428. [CrossRef]
31. Zhou, H.; Liu, J.; Fang, Z.; Zhang, P.; Zhang, B.; Ma, M.; Zeng, J. Control Strategy for Resonant Inverter in High Frequency AC Power Distribution System with Harmonic Suppression and Transient Performance Improvement. *Energies* **2022**, *15*, 8992. [CrossRef]
32. Sahoo, B.; Alhaider, M.M.; Rout, P.K. Effective Harmonic Cancellation Technique for a Three-Phase Four-Wire System. *Energies* **2022**, *15*, 7526. [CrossRef]
33. Park, J.-I.; Park, C.-H. Harmonic Contribution Assessment Based on the Random Sample Consensus and Recursive Least Square Methods. *Energies* **2022**, *15*, 6448. [CrossRef]
34. Afonso, J.L.; Silva, H.J.R.; Martins, J.S. *Active Filters for Power Quality Improvement*; IEEE Porto Powertech: Porto, Portugal, 2001; pp. 1–8.
35. Afonso, J.L.; Aredes, M.; Watanabe, E.H.; Martins, J.S. *Shunt Active Filter for Power Quality Improvement*; International Conference User Interface Engineering: Lisboa, Portugal, 2000; pp. 683–691.
36. Mannen, T.; Fukasawa, I.; Fujita, H. A New Control Method of Suppressing DC Capacitor Voltage Ripples Caused by Third-Order Harmonic Compensation in Three-Phase Active Power Filters. *IEEE Trans. Ind. Appl.* **2018**, *54*, 6149–6158. [CrossRef]
37. Akagi, H.; Kanazawa, Y.; Nabae, A. Generalized Theory of the Instantaneous Reactive Power in Three-PhaseCircuits, In Proceedings of the IPEC'83—Int. Power Electronics Conf. Tokyo, Japan; 1983; pp. 1375–1386.
38. Akagi, H.; Kanazawa, Y.; Nabae, A. Instanataneous Reactive Power Compensator Comprising Switching Devices without Energy Storage Compenents. *IEEE Trans. Industry Applic.* **1984**, *3*, 625–630. [CrossRef]
39. Afonso, J.L.; Couto, C.; Martins, J. *Active Filters with Control Based on the p-q Theory*; IEEE Industrial Electronics Society Newsletter: New York, NY, USA, 2000; pp. 5–10. ISSN 0746-1240. Available online: https://core.ac.uk/download/pdf/55603571.pdf (accessed on 22 January 2023).
40. Afonso, J.L.; Freitas, M.J.S.; Martins, J.S. *p-q Theory Power Components Calculations*; ISIE'2003—IEEE International Symposium on Industrial Electronics: Rio de Janeiro, Brasil, 2003; ISBN 0-7803-7912-8.
41. McLymann, C.W.T. *Transformer and Inductor Design Handbook*, 3rd ed.; CRC Press: New York, NY, USA, 2004; ISBN 0824753933.
42. Pregitzer, R.; Costa, J.C.; Martins, J.S.; Afonso, J.L. Simulation and implementation of a 3-phase 4-wire shunt active power filter. In Proceedings of the 6th International Conference on Harmonics and Power Quality, Cascais, Portugal, 1–5 October 2006; pp. 1–6.

Disclaimer/Publisher's Note: The statements, opinions and data contained in all publications are solely those of the individual author(s) and contributor(s) and not of MDPI and/or the editor(s). MDPI and/or the editor(s) disclaim responsibility for any injury to people or property resulting from any ideas, methods, instructions or products referred to in the content.